Additional file 1: Supplementary Figures

Article Title:

Enhanced B7-H4 expression in gliomas with low PD-L1 expression identifies super-cold tumors

Authors:

Di Chen[1], Gaopeng Li[2], Chunxia Ji[3], Qiqi Lu[3], Ying Qi[1], Chao Tang[1, 3], Ji Xiong[4], Jian Hu[5], Fatma Betul Aksoy Yasar[5], Yan Zhang[2], Dave S.B. Hoon[6], Yu Yao[1], Liangfu Zhou[1, 3]

Affiliations:

1   Department of Neurosurgery, Huashan hospital, Fudan University, Shanghai, China

2   Shenzhen Key Laboratory of Marine Bioresources and Ecology, Brain Disease and Big Data Research Institute, College of Life Sciences & and Oceanography, Shenzhen University, Shenzhen, Guangdong, China

3   Neurosurgical Immunology Laboratory, Neurosurgical Institute of Fudan University，Shanghai , China

4   Department of Pathology, Huashan hospital, Fudan University, Shanghai, China

5   Department of Cancer Biology, University of Texas MD Anderson Cancer Center, Houston, TX, USA

6   Department of Translational Molecular Medicine, John Wayne Cancer Institute, Providence Health Systems, Santa Monica, CA, USA
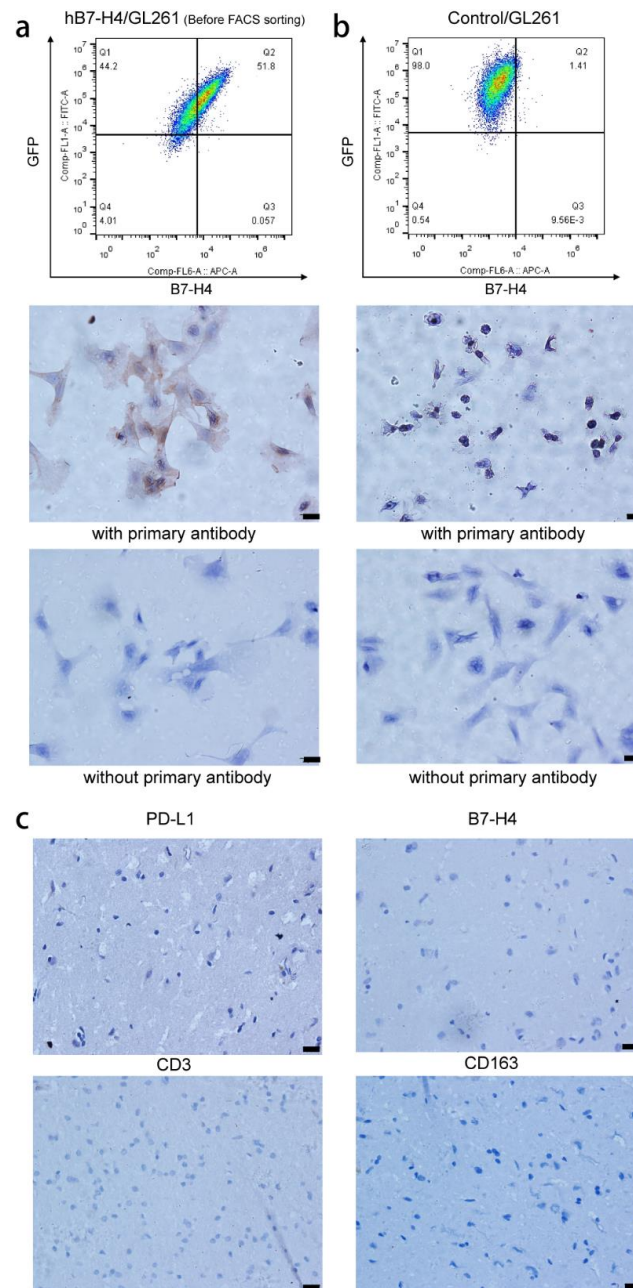
Fig. S1. Quality control slides for antibodies used in IHC. Flow cytometry (B7-H4 Ab, clone#2319B, R&D Systems) and IHC (B7-H4 Ab, ab209242, Abcam) for GL261 cells transfected with human B7-H4 gene **(a).** Flow cytometry and IHC for GL261 cells transfected with an empty vector **(b).** IHC in normal brain tissues **(c).** Magnification, 40x objective; Bar, 20um.
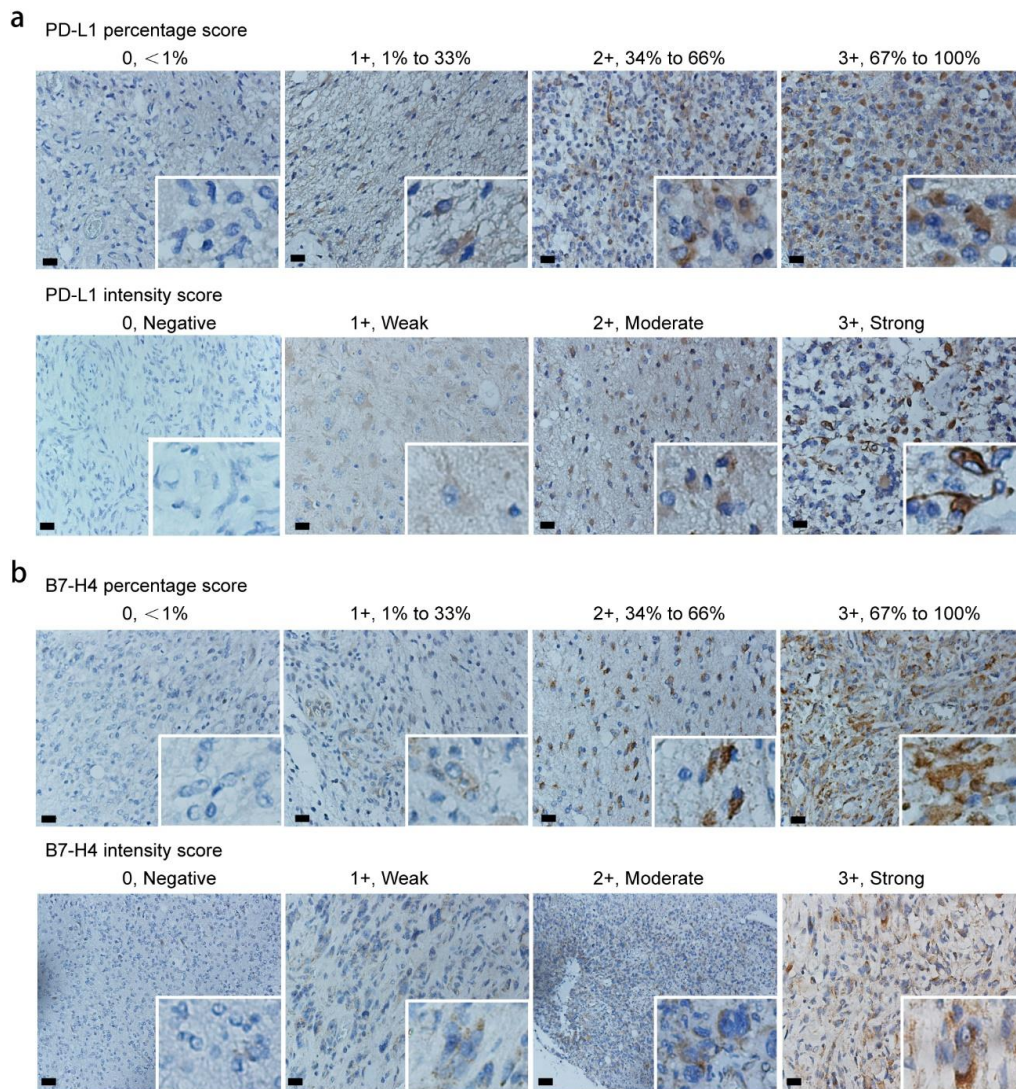
Fig. S2. Representative specimens demonstrating varying IHC scores of PD-L1 and B7-H4. Percentage and intensity score in PD-L1 staining **(a)**. Percentage and intensity score in B7-H4 staining **(b)**. Magnification, 40x objective; Bar, 20um.
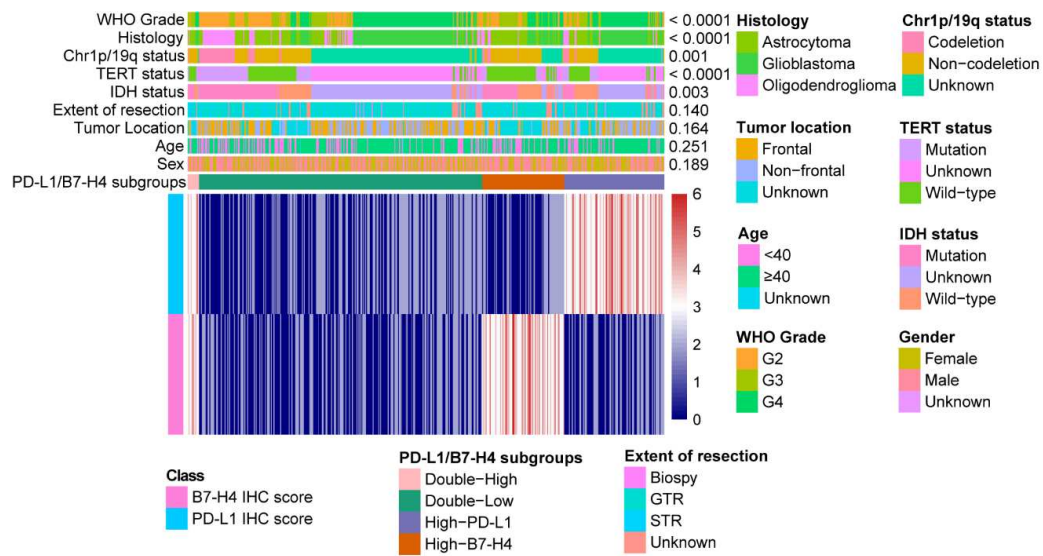
Fig. S3. Distributions of different clinicopathologic parameters in PD-L1/B7-H4 subgroups (examined with Fisher's exact test).
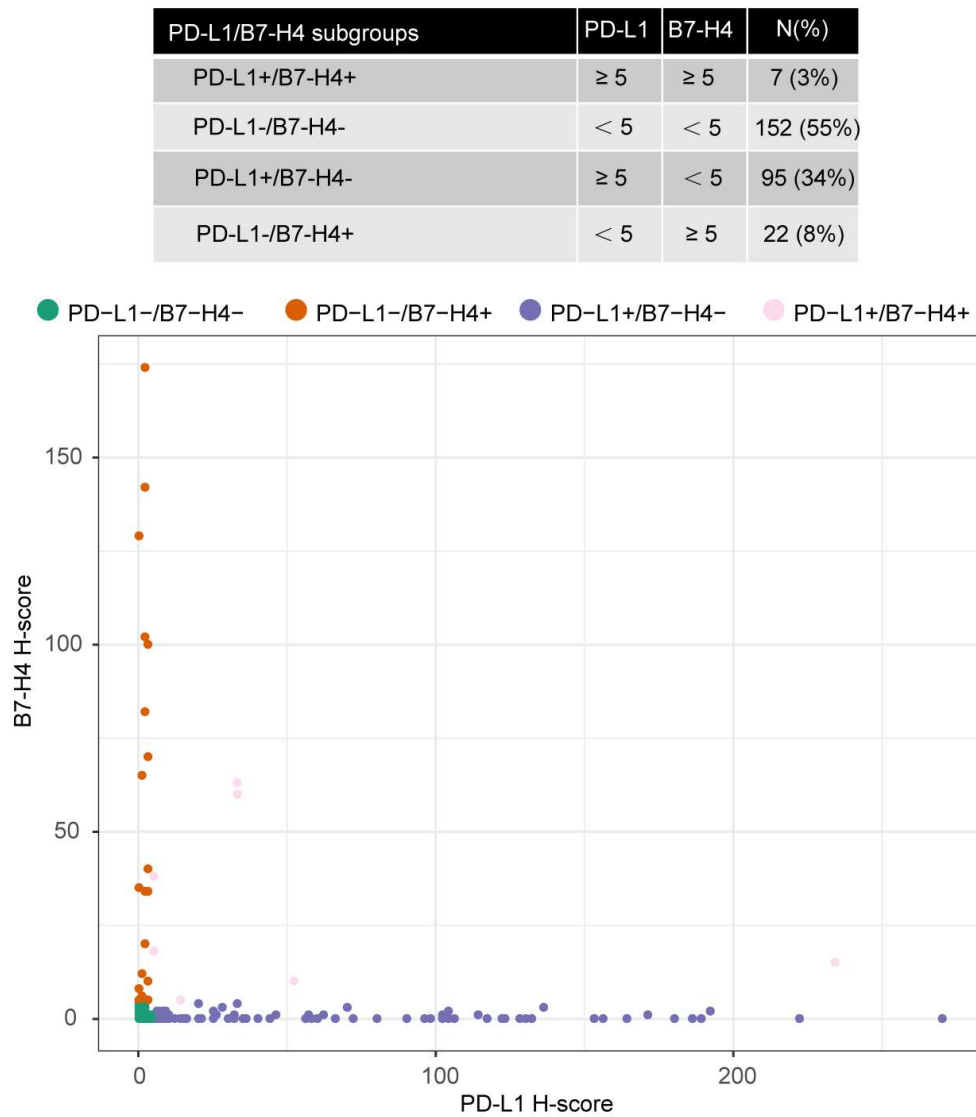
PD-L1/B7-H4 subgroups	PD-L1	B7-H4	N(%)
PD-L1+/B7-H4+	≥ 5	≥ 5	7 (3%)
PD-L1-/B7-H4-	< 5	< 5	152 (55%)
PD-L1+/B7-H4-	≥ 5	< 5	95 (34%)
PD-L1-/B7-H4+	< 5	≥ 5	22 (8%)

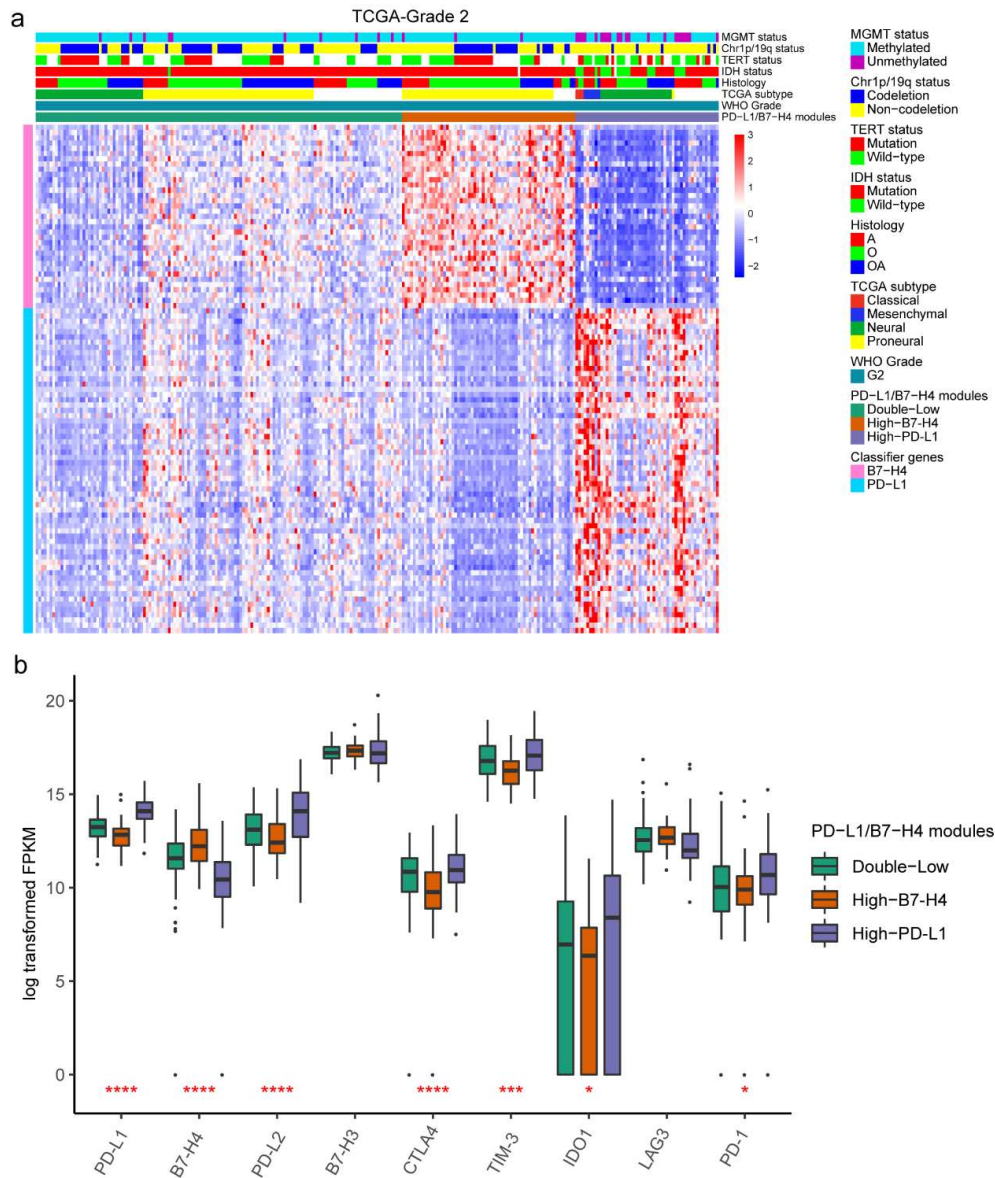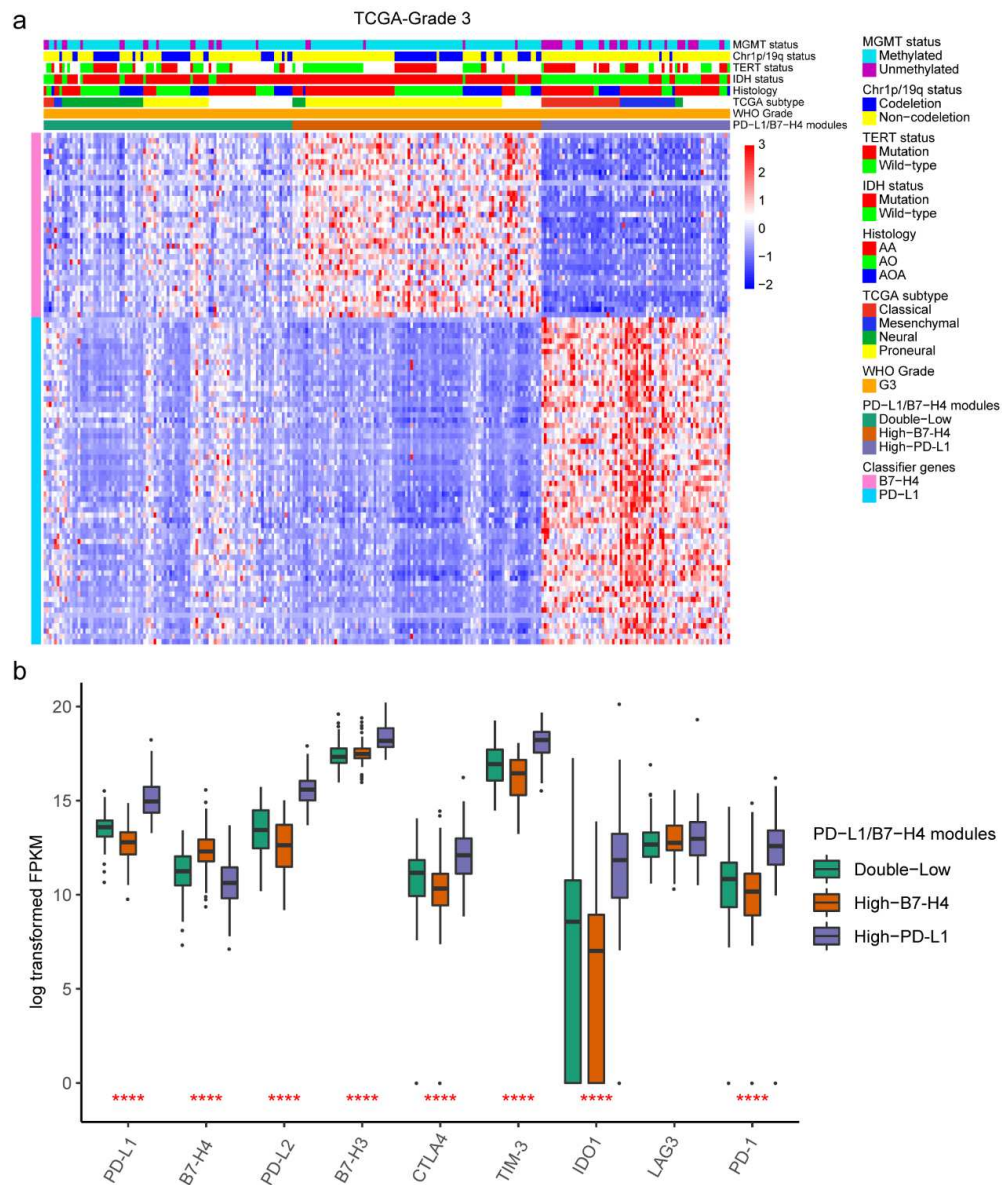**Fig. S4.** Correlation between PD-L1 and B7-H4 expression (cutoff of H-score = 5).

Fig. S5. Gene co-expression modules in the grade 2 gliomas from TCGA dataset showed mutually exclusive expression profiles. Gene co-expression modules using PD-L1/B7-H4 classifier genes **(a)**. mRNA expression distribution of estimable checkpoint molecules among PD-L1/B7-H4 modules, including PD-L1 and B7-H4 **(b)**.
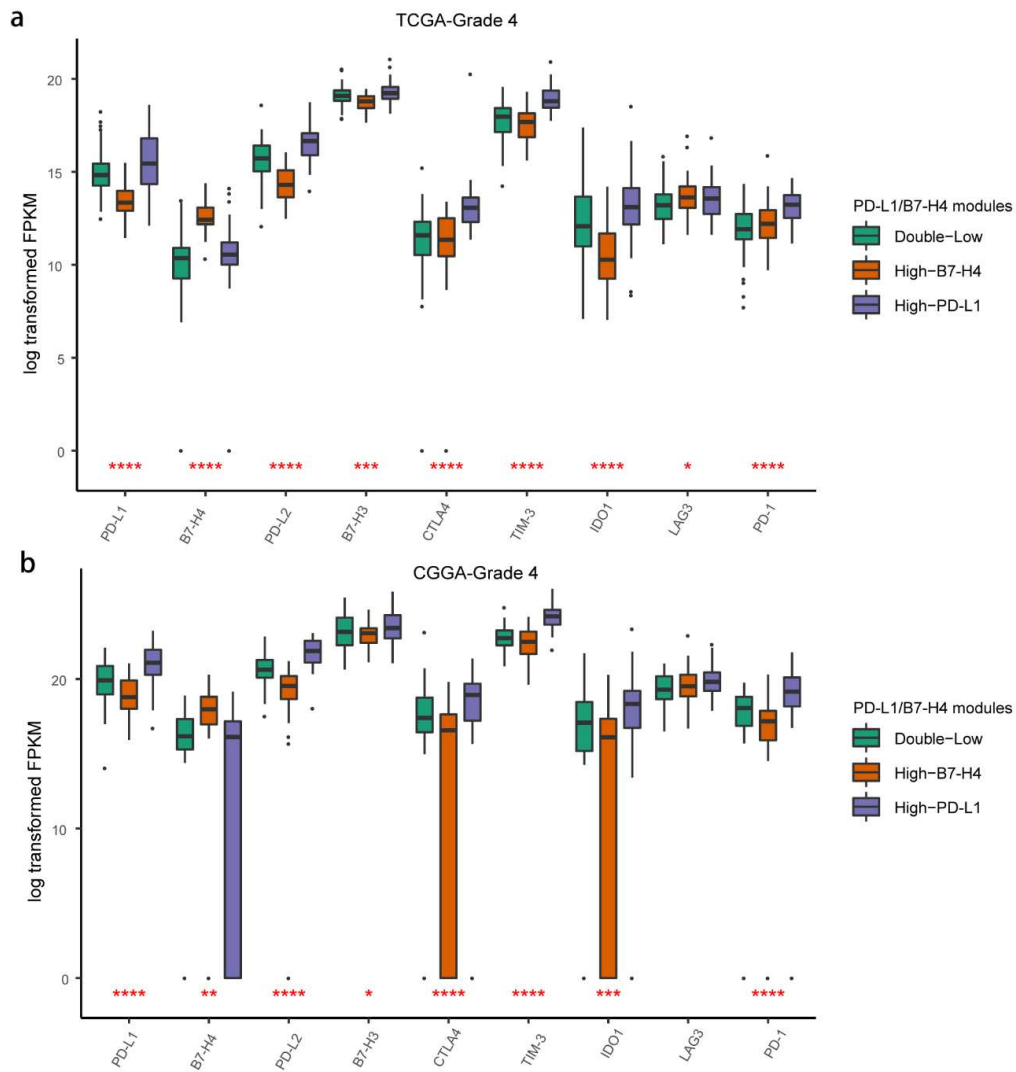
Fig. S6. Gene co-expression modules in the grade 3 gliomas from TCGA dataset showed mutually exclusive expression profiles. Gene co-expression modules using PD-L1/B7-H4 classifier genes **(a)**. mRNA expression distribution of estimable checkpoint molecules among PD-L1/B7-H4 modules, including PD-L1 and B7-H4 **(b)**.

Fig. S7. mRNA expression distribution of estimable checkpoint molecules among PD-L1/B7-H4 modules in grade 4 gliomas from RNA-seq datasets. Grade 4 gliomas in TCGA dataset **(a)**. Grade 4 gliomas in CGGA dataset **(b)**.
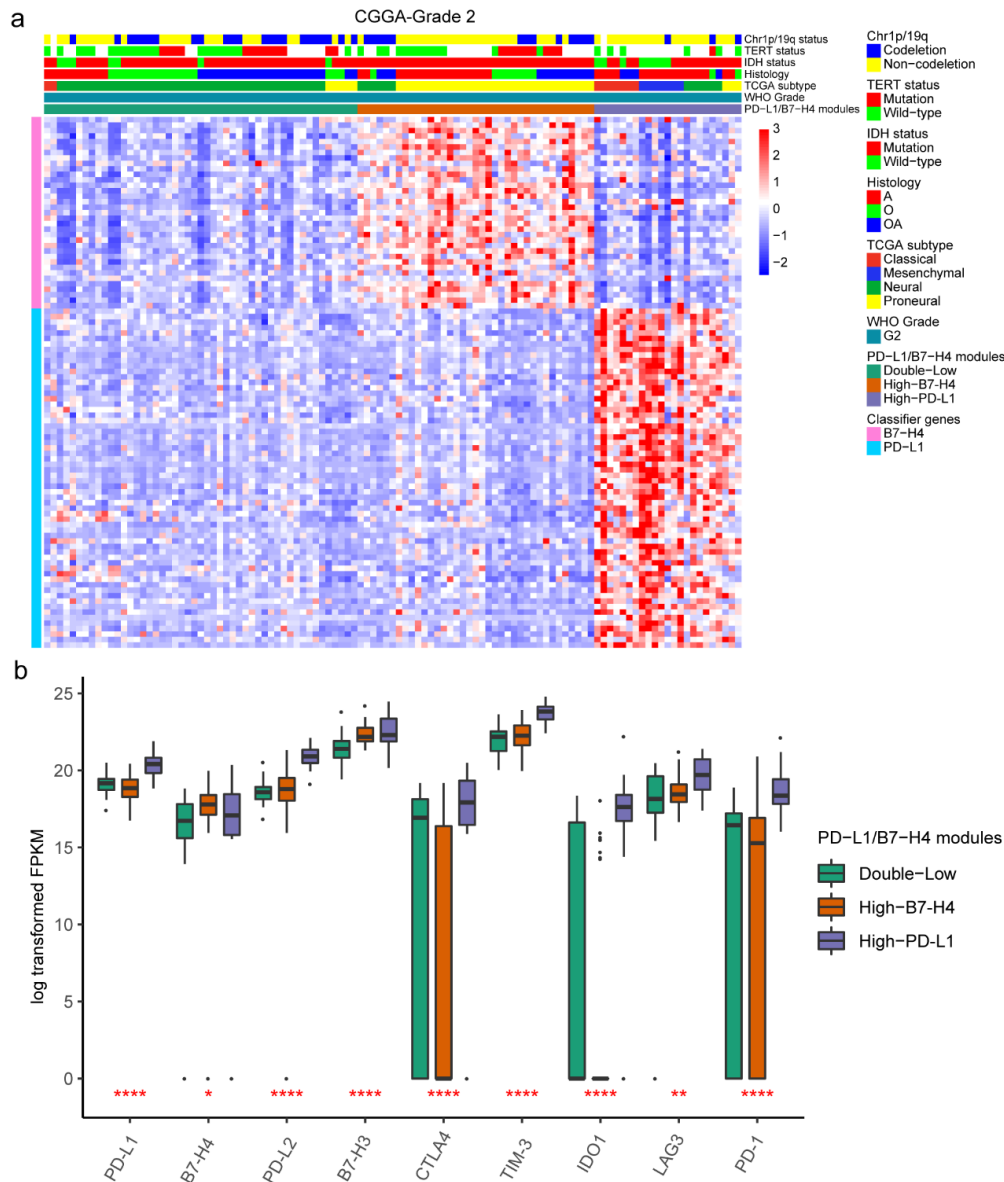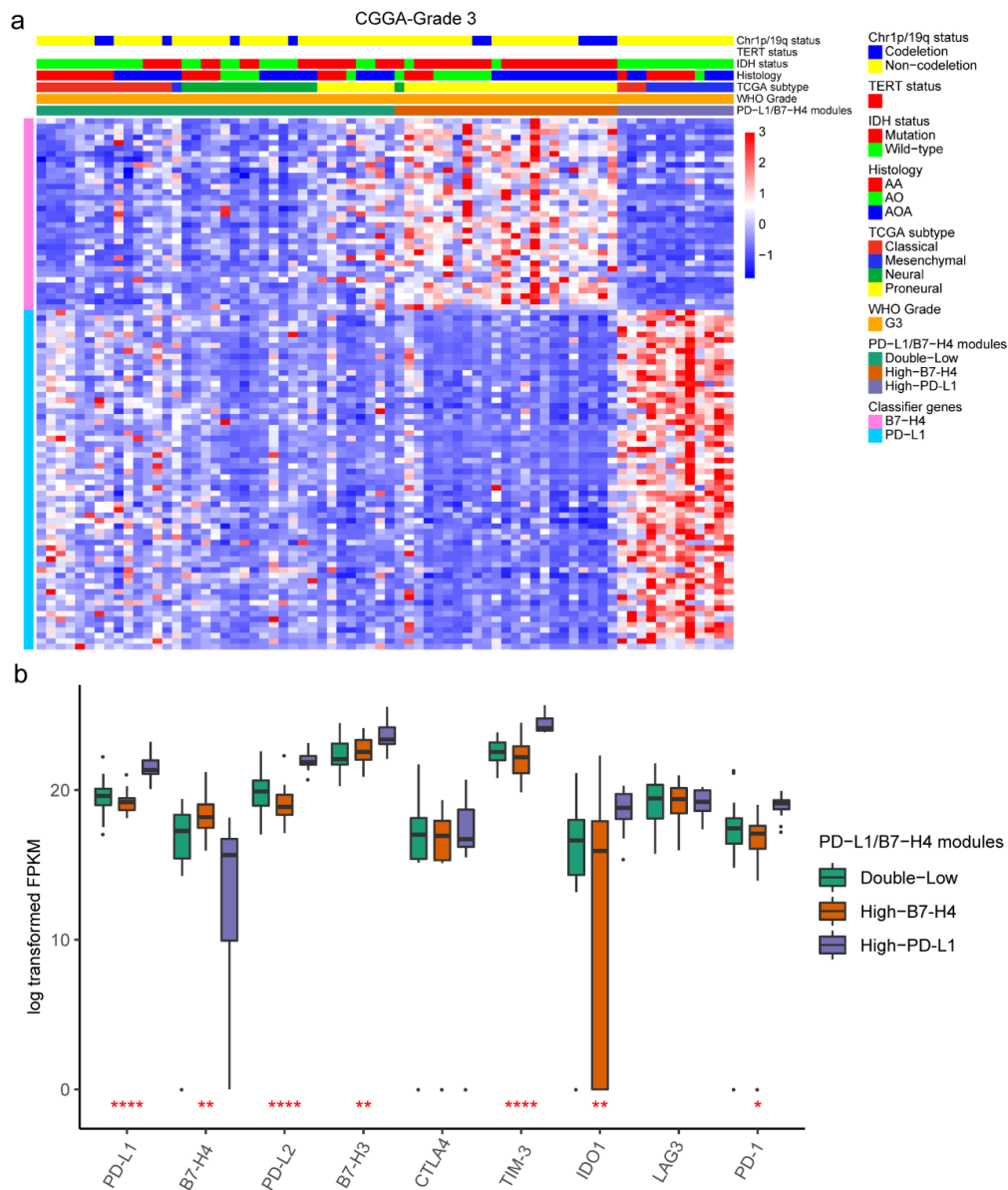
Fig. S8. Gene co-expression modules in the grade 2 gliomas from CGGA dataset showed mutually exclusive expression profiles. Gene co-expression modules using PD-L1/B7-H4 classifier genes **(a)**. mRNA expression distribution of estimable checkpoint molecules among PD-L1/B7-H4 modules, including PD-L1 and B7-H4 **(b)**.

Fig. S9. Gene co-expression modules in the grade 3 gliomas from CGGA dataset showed mutually exclusive expression profiles. Gene co-expression modules using PD-L1/B7-H4 classifier genes **(a)**. mRNA expression distribution of estimable checkpoint molecules among PD-L1/B7-H4 modules, including PD-L1 and B7-H4 **(b)**.
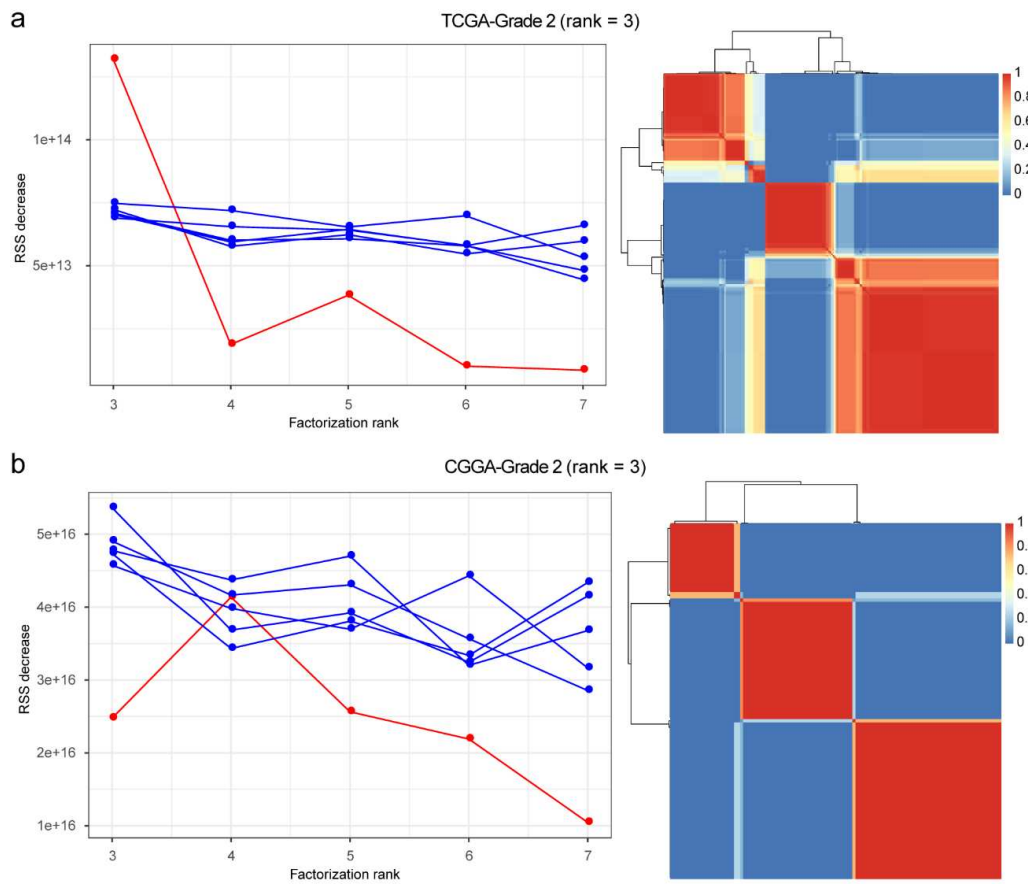
J Immunother Cancer

Fig. S10. Identification of PD-L1/B7-H4 modules in grade 2 gliomas from RNA-seq

datasets. TCGA dataset (rank=3) **(a)**. CGGA dataset (rank=3) **(b)**.
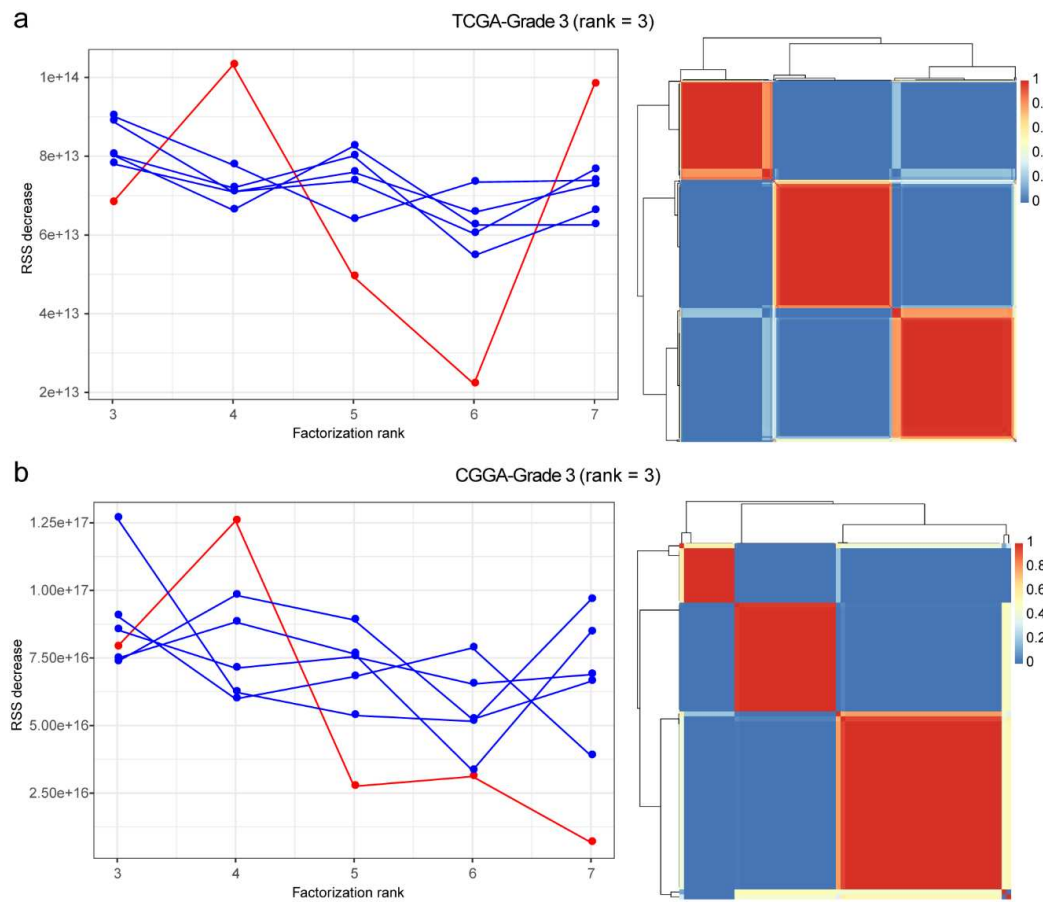
Fig. S11. Identification of PD-L1/B7-H4 modules in grade 3 gliomas from RNA-seq

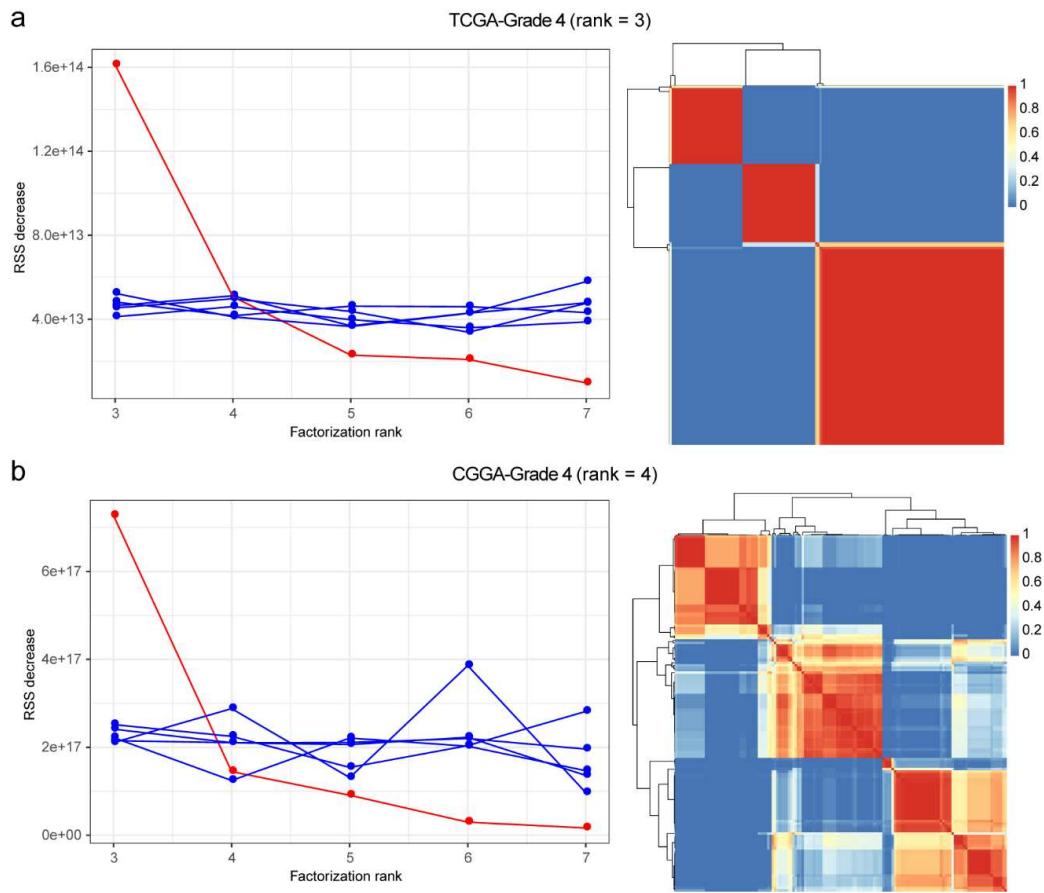datasets. TCGA dataset (rank=3) **(a)**. CGGA dataset (rank=3) **(b)**.

Fig. S12. Identification of PD-L1/B7-H4 modules in grade 4 gliomas from RNA-seq

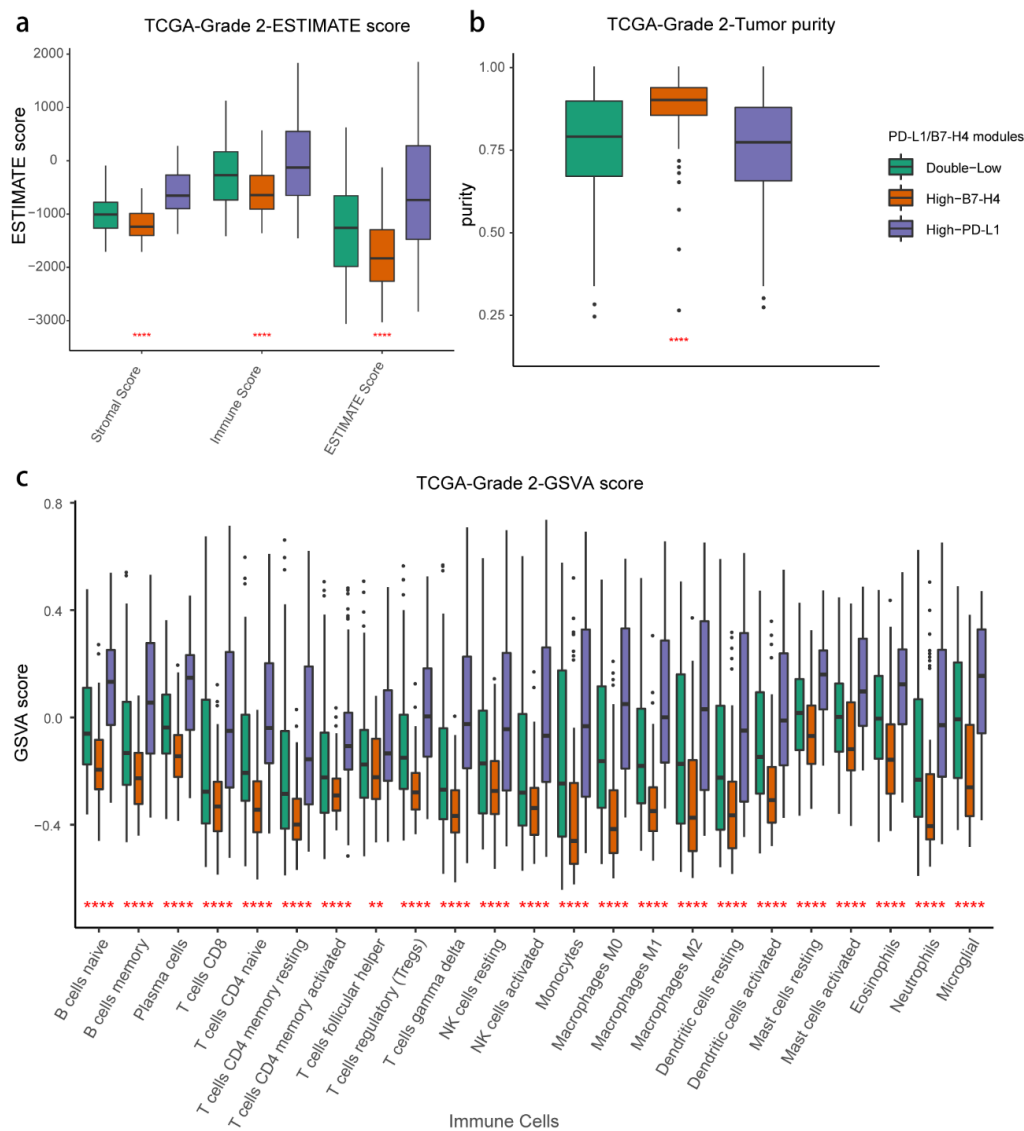datasets. TCGA dataset (rank=3) **(a)**. CGGA dataset (rank=4) **(b)**.

Fig. S13. Assessment of tumor immune microenvironment among PD-L1/B7-H4 modules in grade 2 gliomas from TCGA dataset. ESTIMATE evaluation showed less immune infiltration in High-B7-H4 module **(a)**. High-B7-H4 module gliomas showed higher tumor purity **(b)**. Comparison of GSVA score representing extent of immune cells infiltration among modules demonstrated lacking immune cells in High-B7-H4 modules **(c)**.
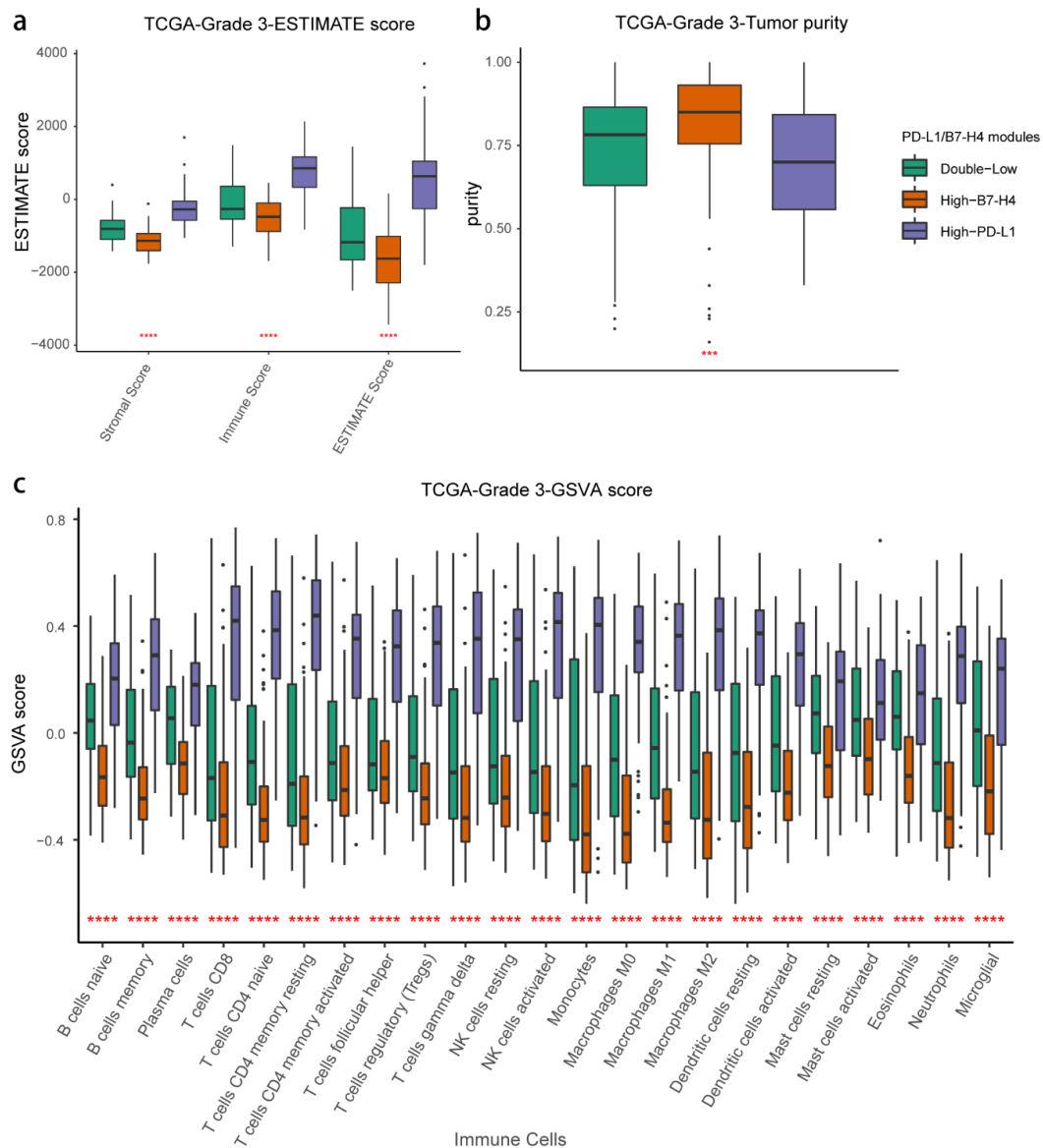
Fig. S14. Assessment of tumor immune microenvironment among PD-L1/B7-H4 modules in grade 3 gliomas from TCGA dataset. ESTIMATE evaluation showed less immune infiltration in High-B7-H4 module **(a)**. High-B7-H4 module gliomas showed higher tumor purity **(b)**. Comparison of GSVA score representing extent of immune cells infiltration among modules demonstrated lacking immune cells in High-B7-H4 modules **(c)**.
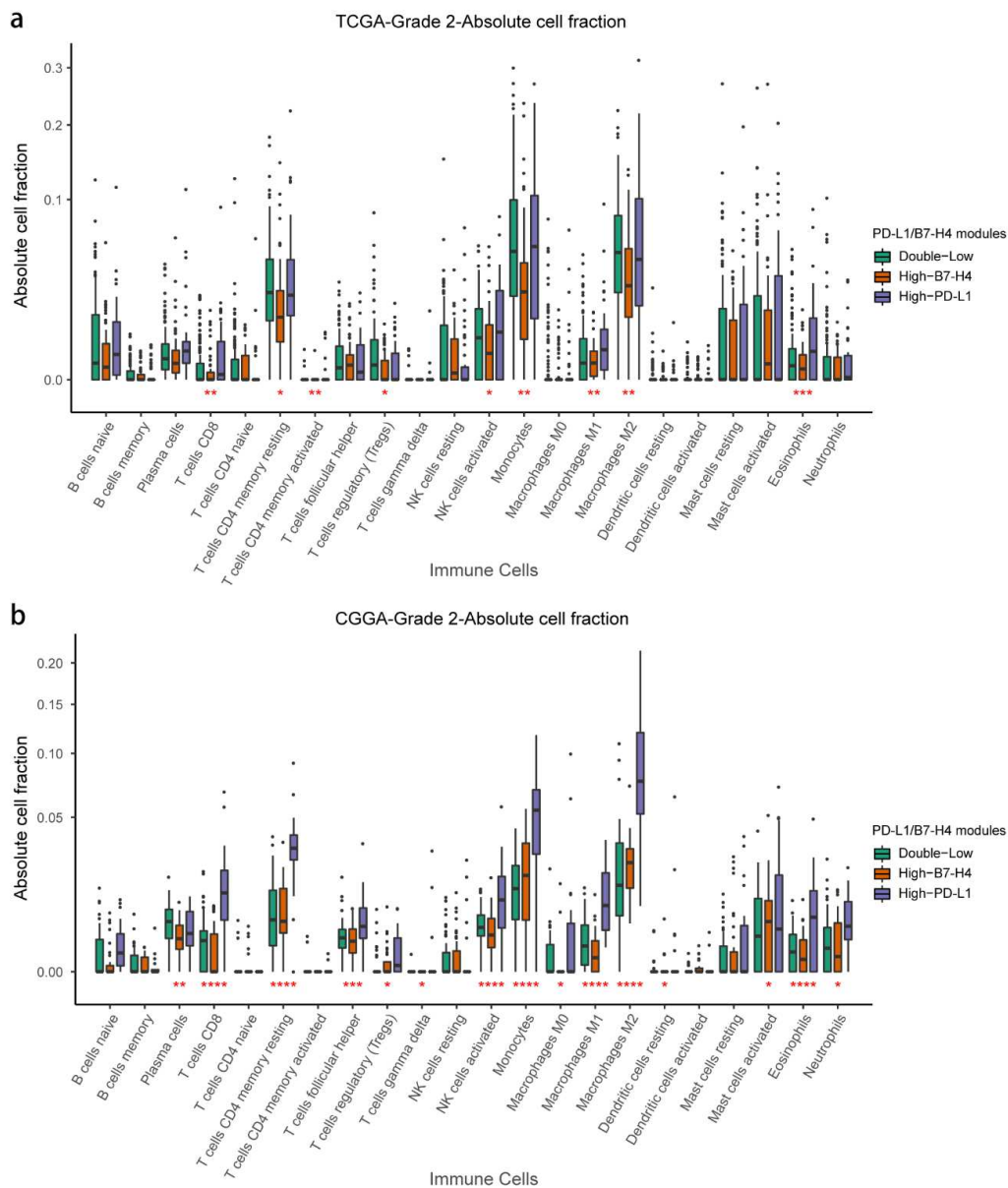
Fig. S15. Absolute immune cell fractions for 22 immune cell populations differed among PD-L1/B7-H4 modules in grade 2 gliomas. Grade 2 gliomas from TCGA dataset **(a)**. Grade 2 gliomas from CGGA dataset **(b)**.
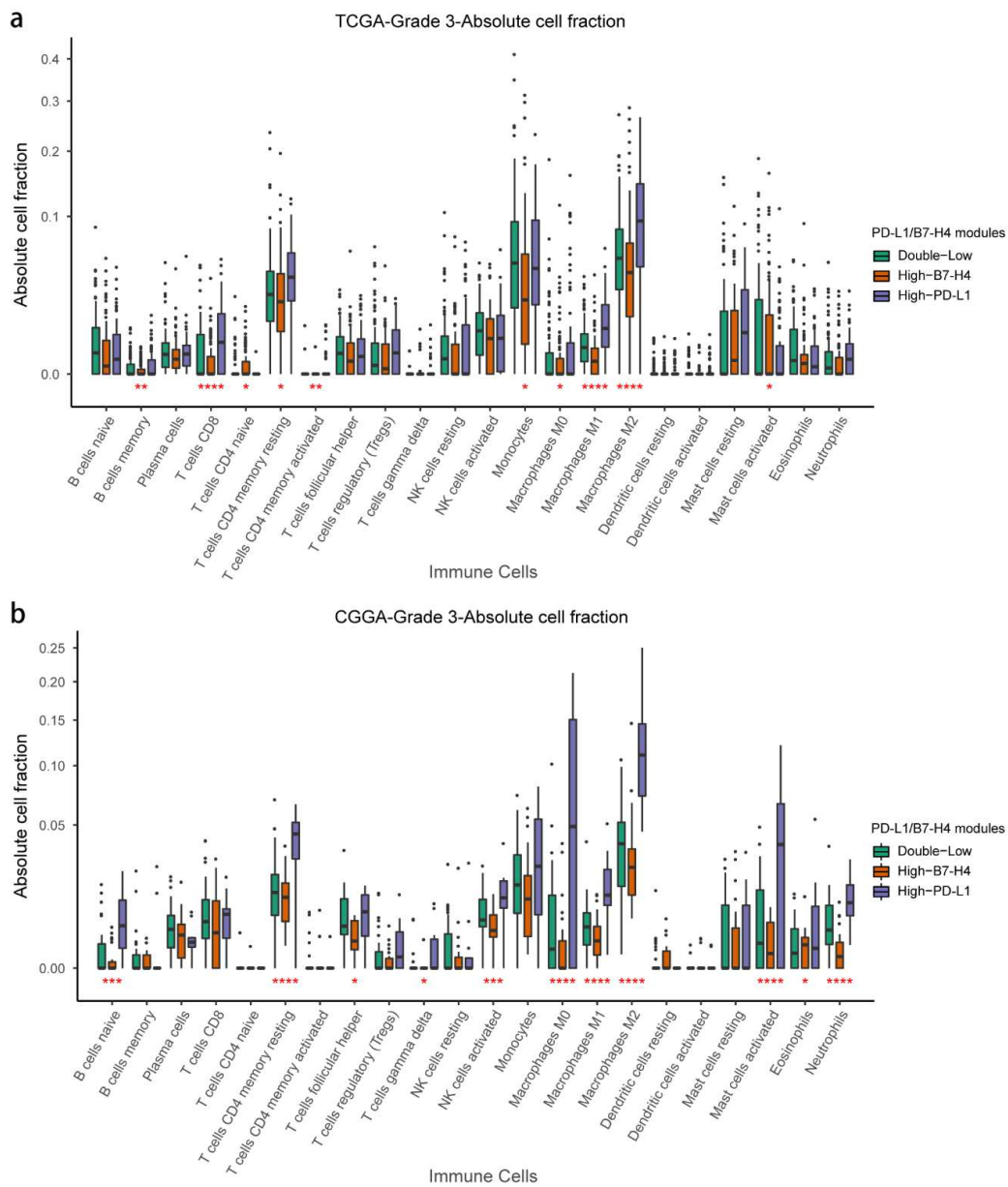
Fig. S16. Absolute immune cell fractions for 22 immune cell populations differed among PD-L1/B7-H4 modules in grade 3 gliomas. Grade 3 gliomas from TCGA dataset **(a)**. Grade 3 gliomas from CGGA dataset **(b)**.
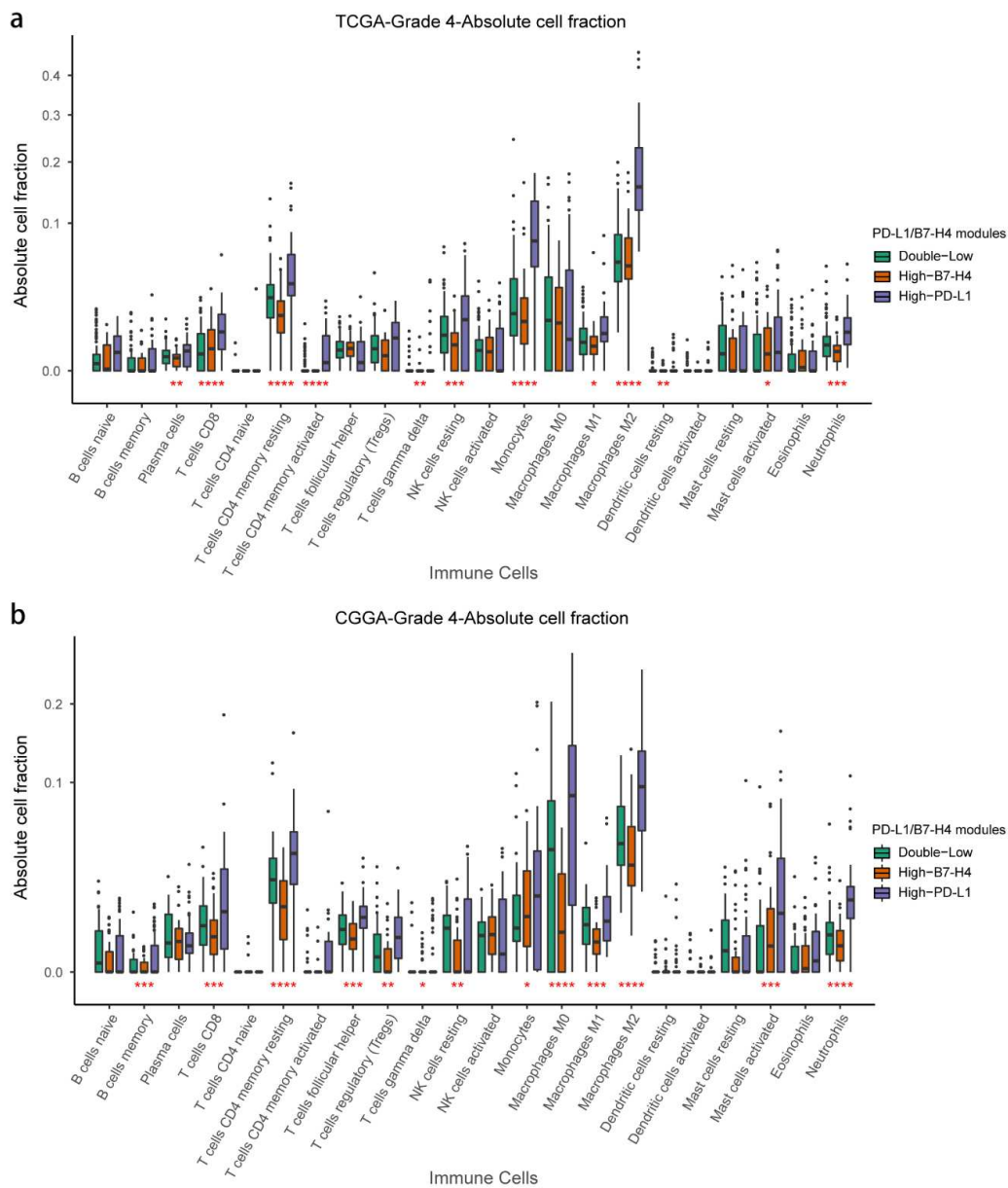
Fig. S17. Absolute immune cell fractions for 22 immune cell populations differed among PD-L1/B7-H4 modules in grade4 gliomas. Grade 4 gliomas from TCGA dataset **(a)**. Grade 4 gliomas from CGGA dataset **(b)**.
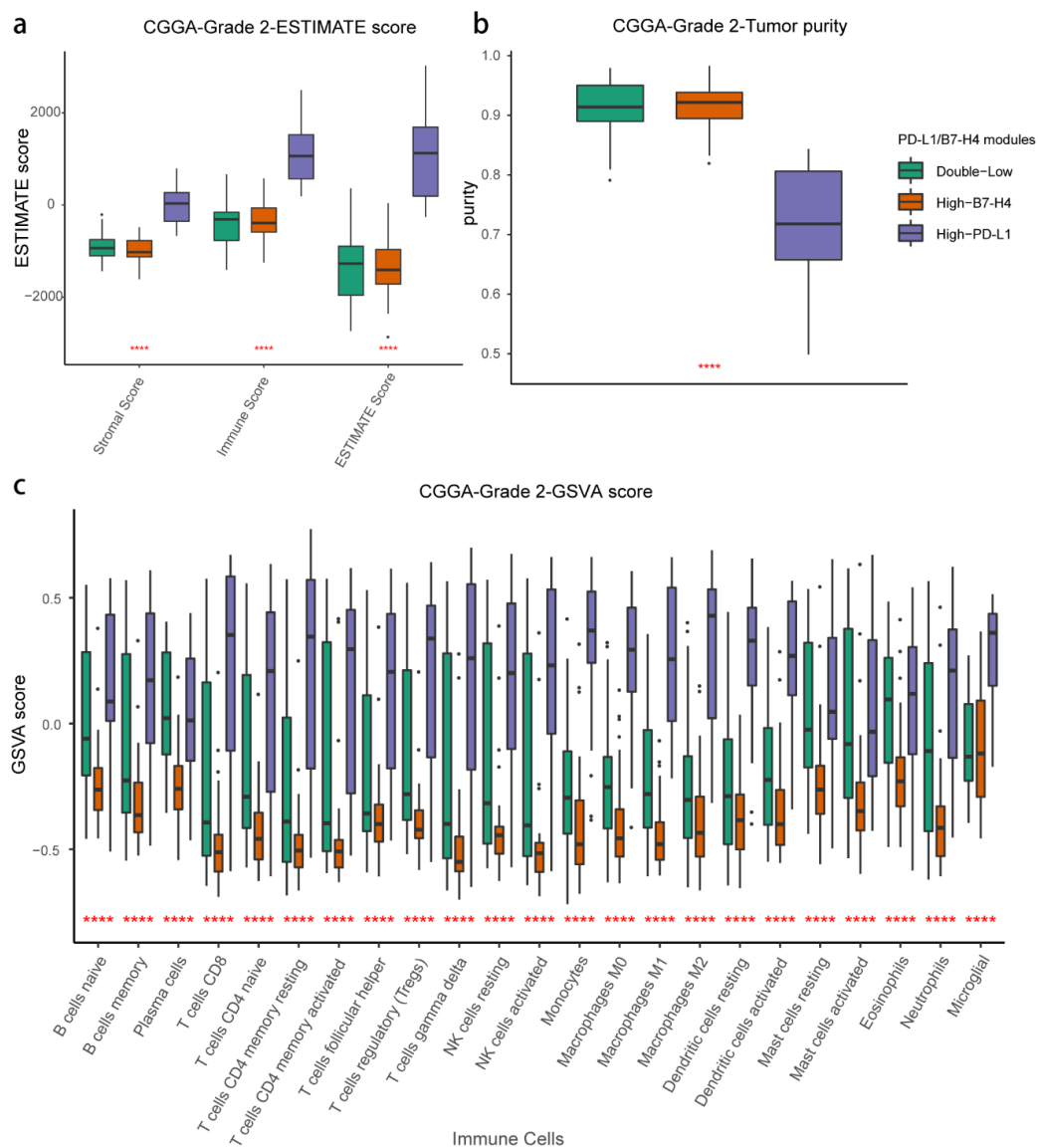
Fig. S18. Assessment of tumor immune microenvironment among PD-L1/B7-H4 modules in grade 2 gliomas from CGGA dataset. ESTIMATE evaluation showed less immune infiltration in High-B7-H4 module **(a)**. High-B7-H4 module gliomas showed higher tumor purity **(b)**. Comparison of GSVA score representing extent of immune cells infiltration among modules demonstrated lacking immune cells in High-B7-H4 modules **(c)**.
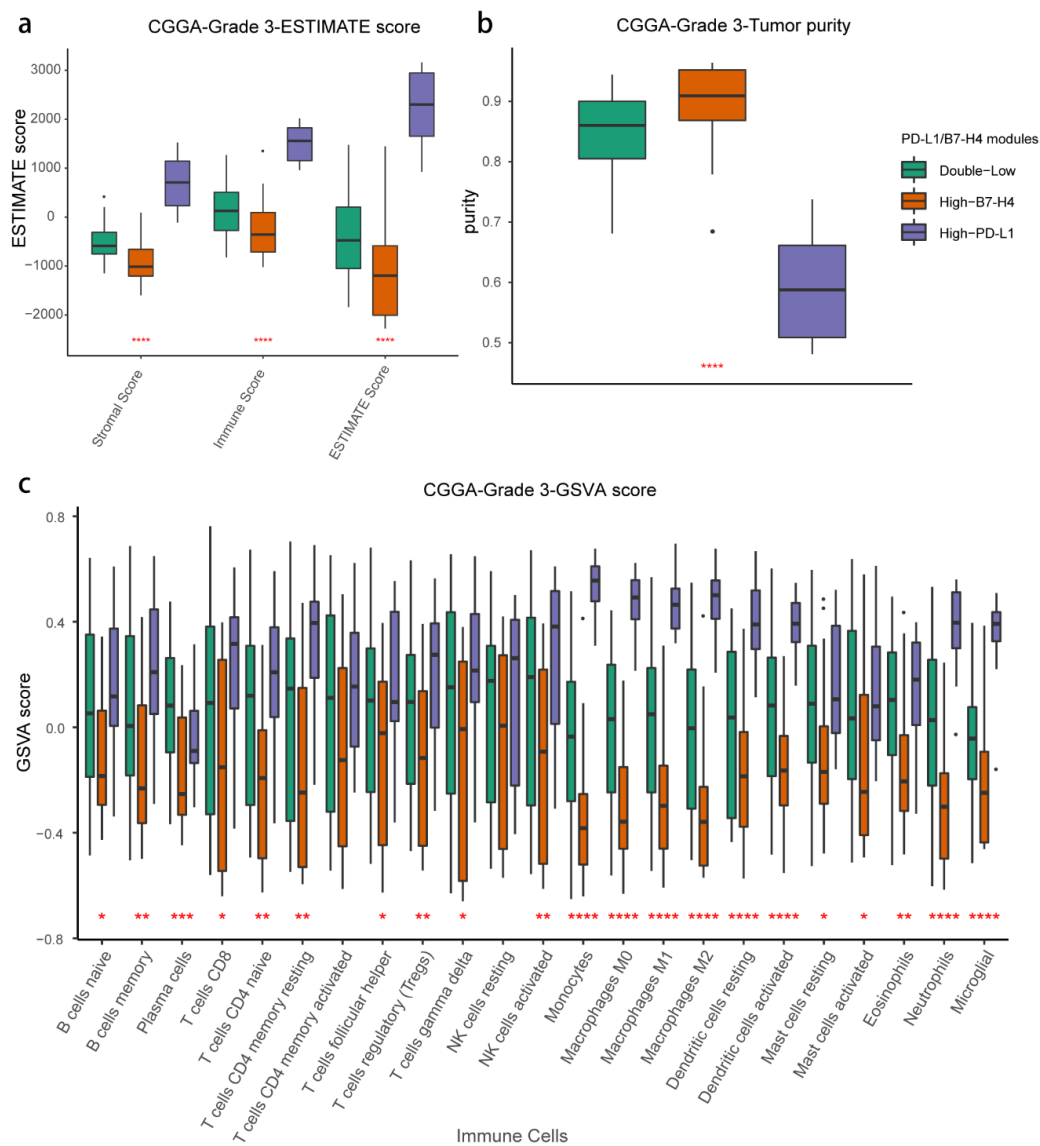
Fig. S19. Assessment of tumor immune microenvironment among PD-L1/B7-H4 modules in grade 3 gliomas from CGGA dataset. ESTIMATE evaluation showed less immune infiltration in High-B7-H4 module **(a)**. High-B7-H4 module gliomas showed higher tumor purity **(b)**. Comparison of GSVA score representing extent of immune cells infiltration among modules demonstrated lacking immune cells in High-B7-H4 modules **(c)**.
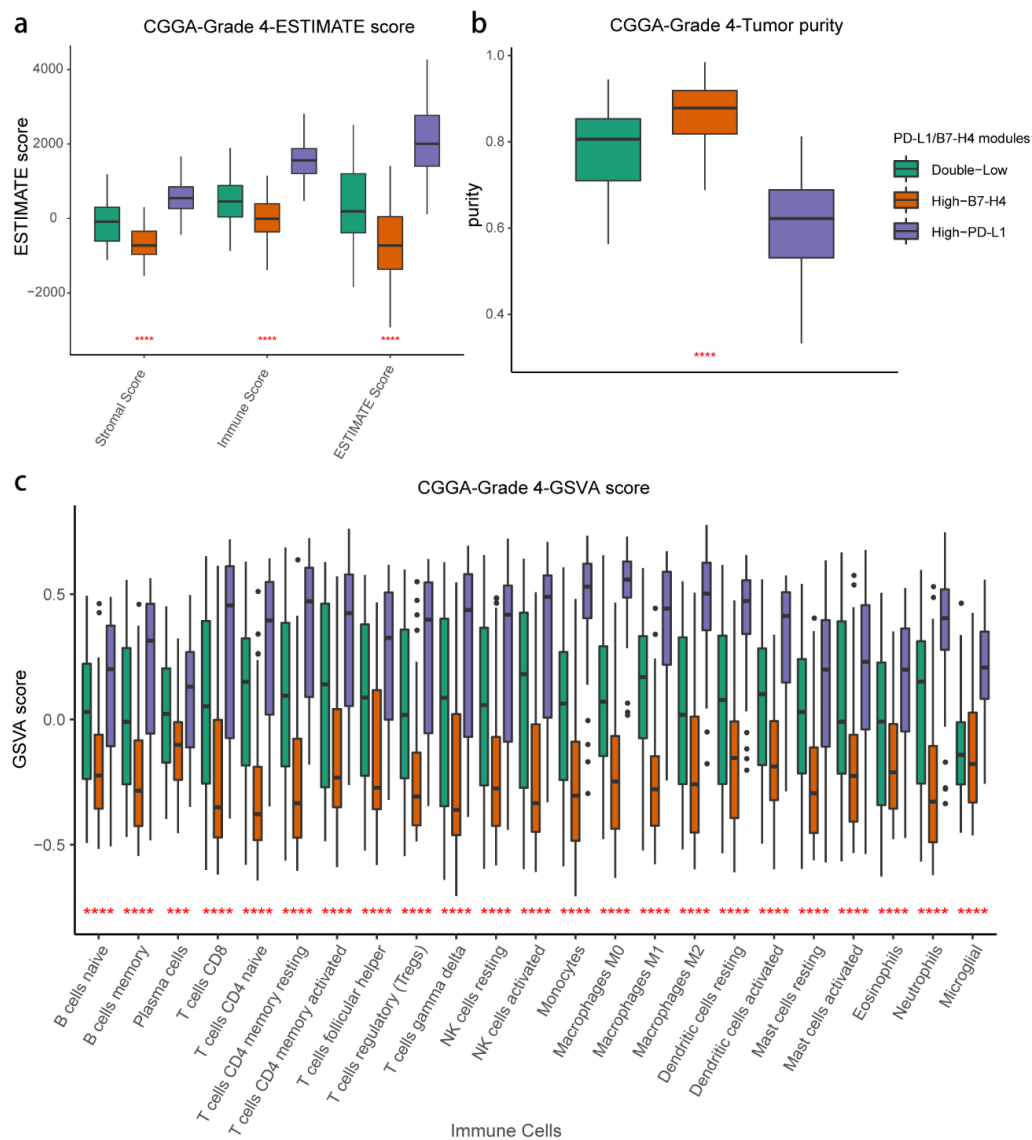
Fig. S20. Assessment of tumor immune microenvironment among PD-L1/B7-H4 modules in grade 4 gliomas from CGGA dataset. ESTIMATE evaluation showed less immune infiltration in High-B7-H4 module **(a)**. High-B7-H4 module gliomas showed higher tumor purity **(b)**. Comparison of GSVA score representing extent of immune cells infiltration among modules demonstrated lacking immune cells in High-B7-H4 modules **(c)**.
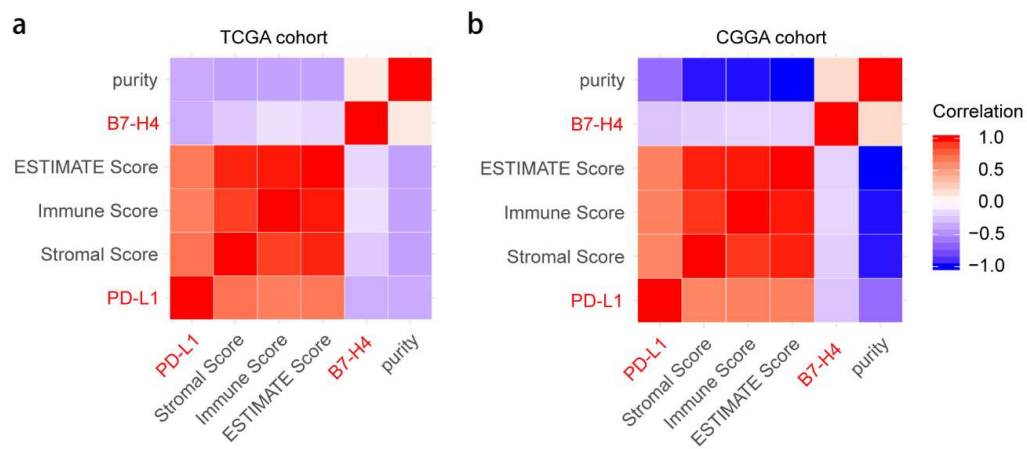
Fig. S21. Correlation analysis among checkpoint molecules and characteristics of immune microenviroment in two RNA-seq datasets showed negative correlation between B7-H4 and extent of immune cell infiltration. The whole cohort from TCGA dataset **(a)**. The whole cohort from CGGA dataset **(b)**.
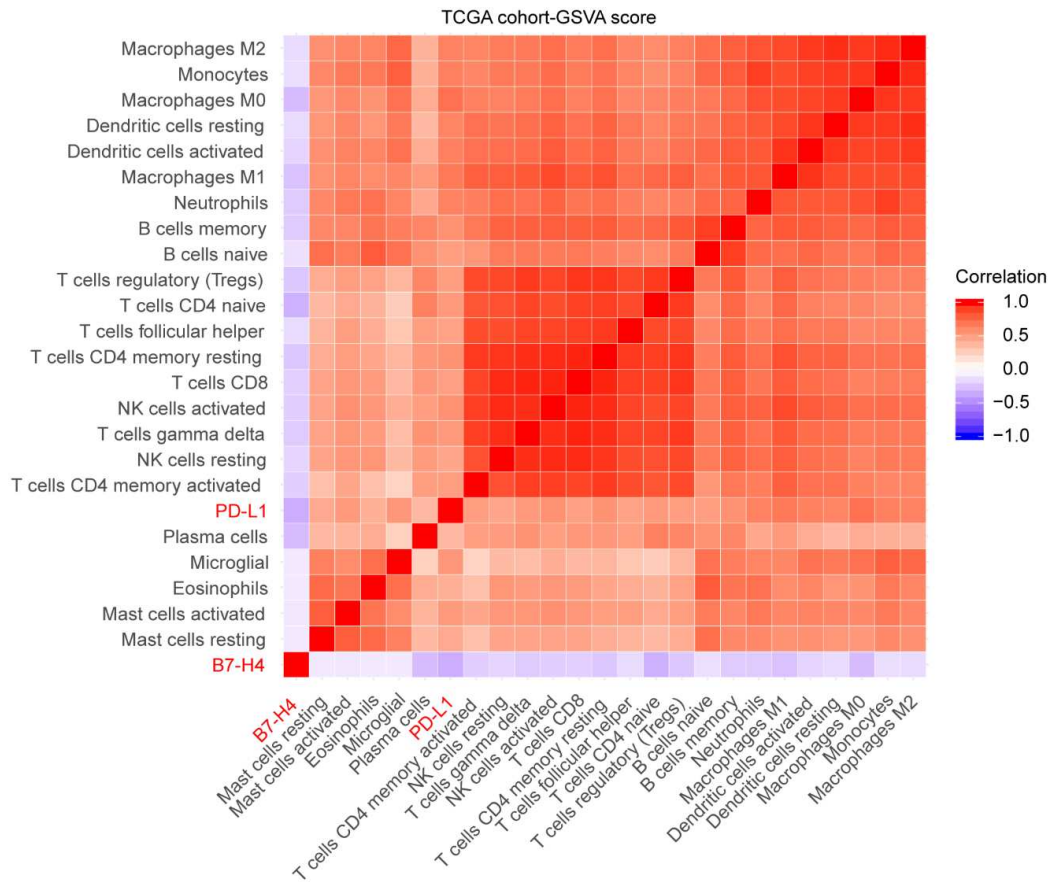
Fig. S22. Correlation analysis among checkpoint molecules and GSVA scores representing the extent of immune cell infiltration in the whole cohort from TCGA dataset showed negative correlation between B7-H4 and extent of immune cell infiltration.
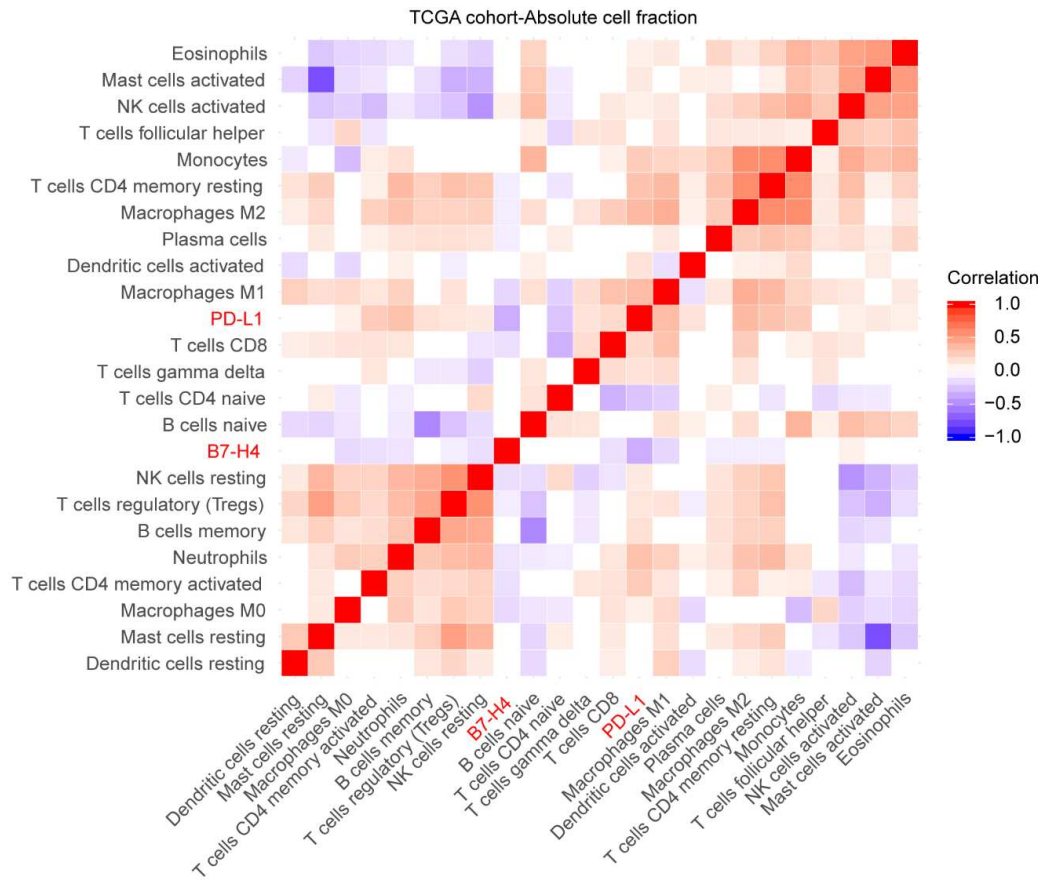
Fig. S23. Correlation analysis among checkpoint molecules and absolute immune cell fractions in the whole cohort from TCGA dataset showed negative correlation between B7-H4 and extent of immune cell infiltration.
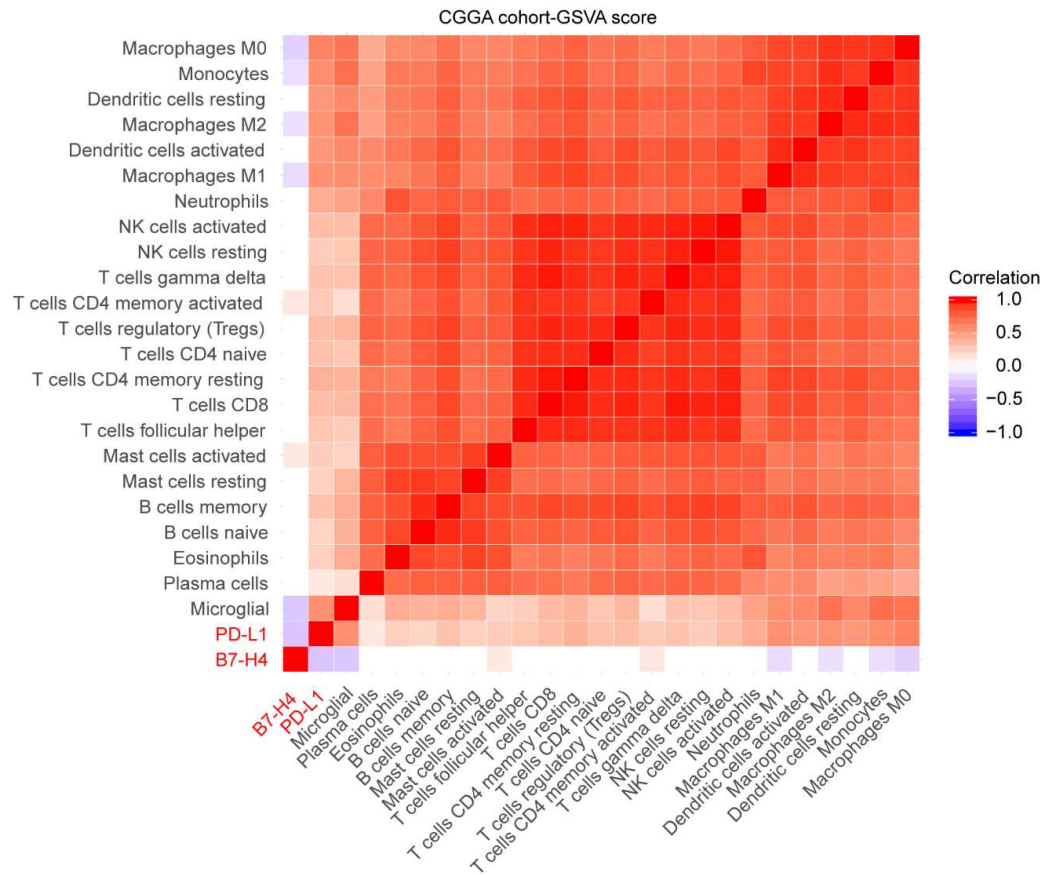
Fig. S24. Correlation analysis among checkpoint molecules and GSVA scores representing the extent of immune cell infiltration in the whole cohort from CGGA dataset showed negative correlation between B7-H4 and extent of immune cell infiltration.
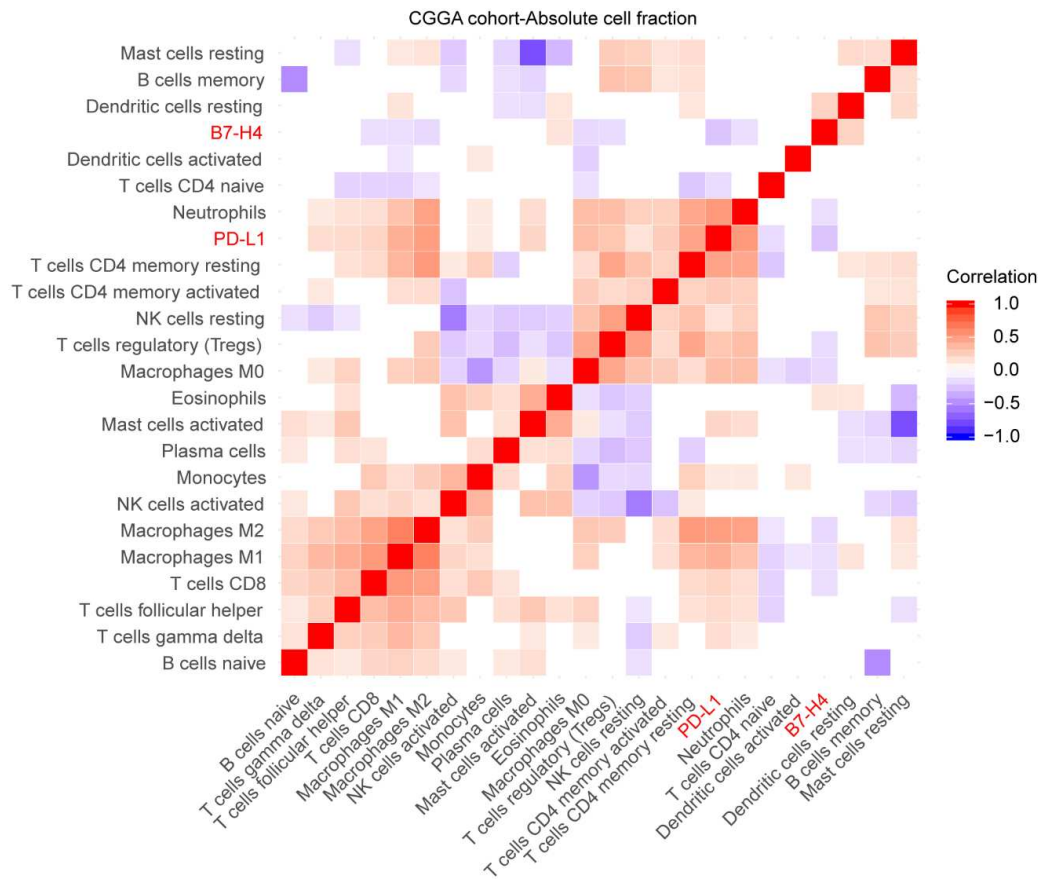
Fig. S25. Correlation analysis among checkpoint molecules and absolute immune cell fractions in the whole cohort from CGGA dataset showed negative correlation between B7-H4 and extent of immune cell infiltration.
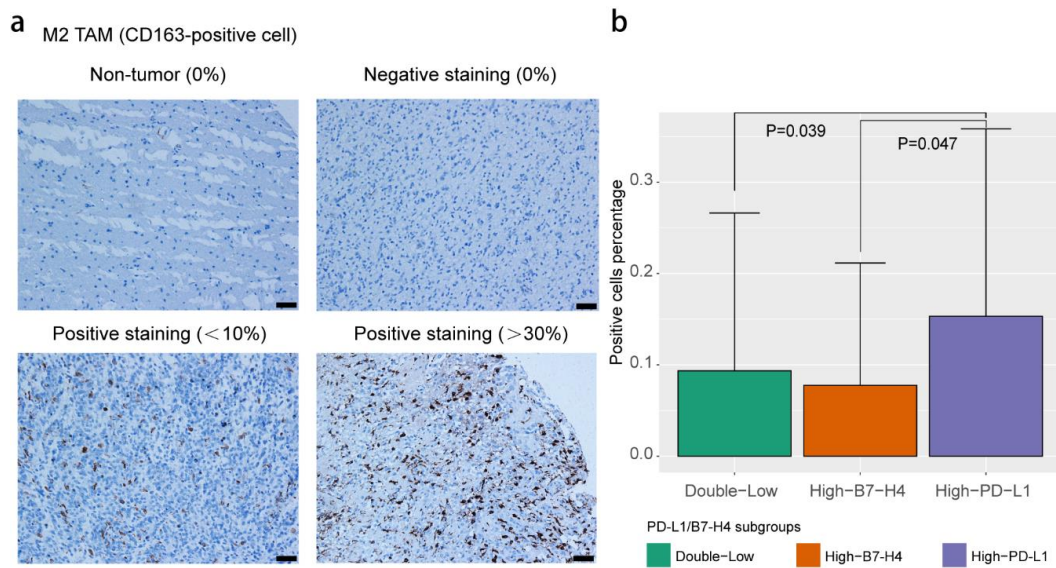
Fig. S26. Difference in TAM (CD163 positive cell) density among PD-L1/B7-H4 subgroup gliomas in TMA cores. Representative examples of TAM infiltration in different extents (**a**). Comparation of positive proportions for CD163 showed High-B7-H4 subgroup gliomas had less TAM infiltration than High-PD-L1 subgroup gliomas (**b**). Magnification, 20x objective; Bar, 50um.
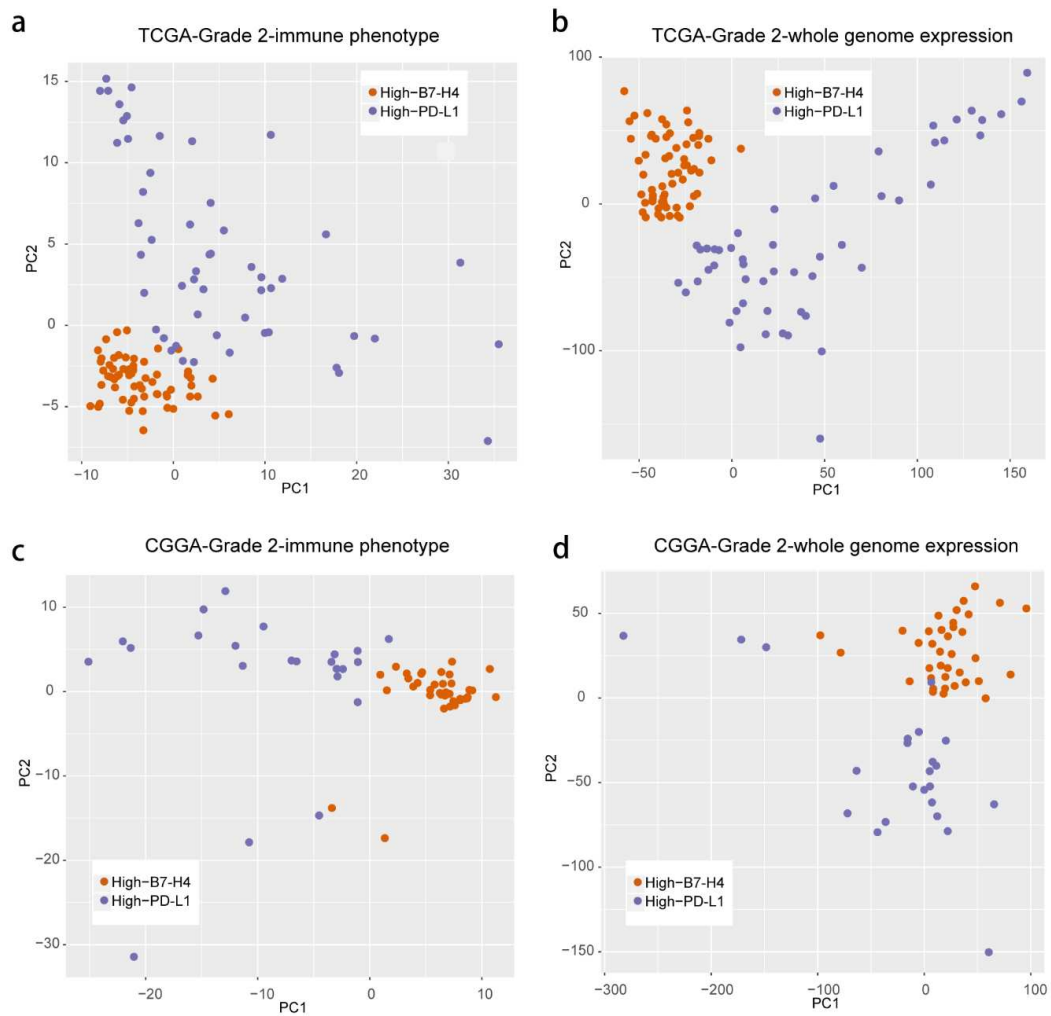
Fig. S27. Principal component analysis between High-PD-L1 and High-B7-H4 modules verified distinct immune phenotypes and whole genome expression profile in grade2 gliomas. Immune phenotype in grade 2 gliomas from TCGA dataset (**a**). Whole genome expression profile in grade 2 gliomas from TCGA dataset (**b**). Immune phenotype in grade 2 gliomas from CGGA dataset (**c**). Whole genome expression profile in grade 2 gliomas from CGGA dataset (**d**).
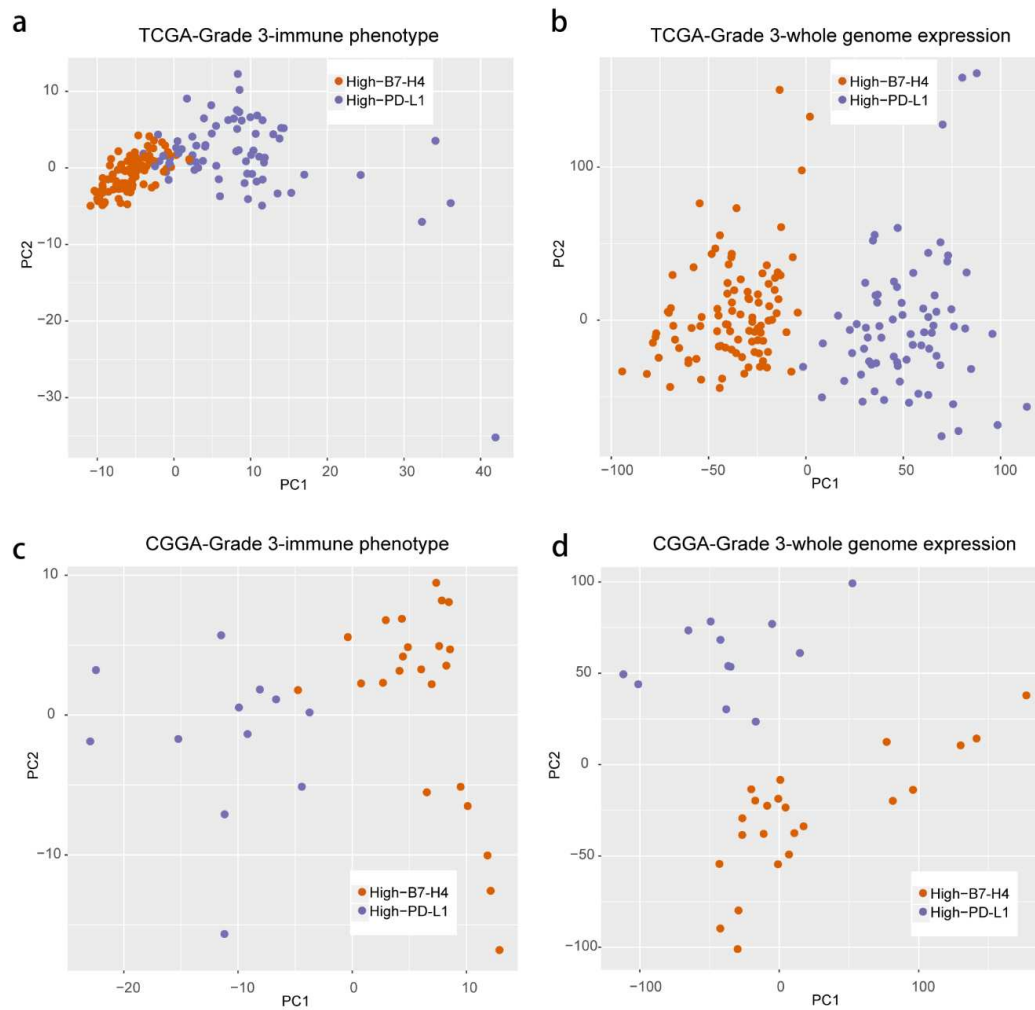
Fig. S28. Principal component analysis between High-PD-L1 and High-B7-H4 modules verified distinct immune phenotypes and whole genome expression profile in grade3 gliomas. Immune phenotype in grade 3 gliomas from TCGA dataset **(a)**. Whole genome expression profile in grade 3 gliomas from TCGA dataset **(b)**. Immune phenotype in grade 3 gliomas from CGGA dataset **(c)**. Whole genome expression profile in grade 3 gliomas from CGGA dataset **(d)**.
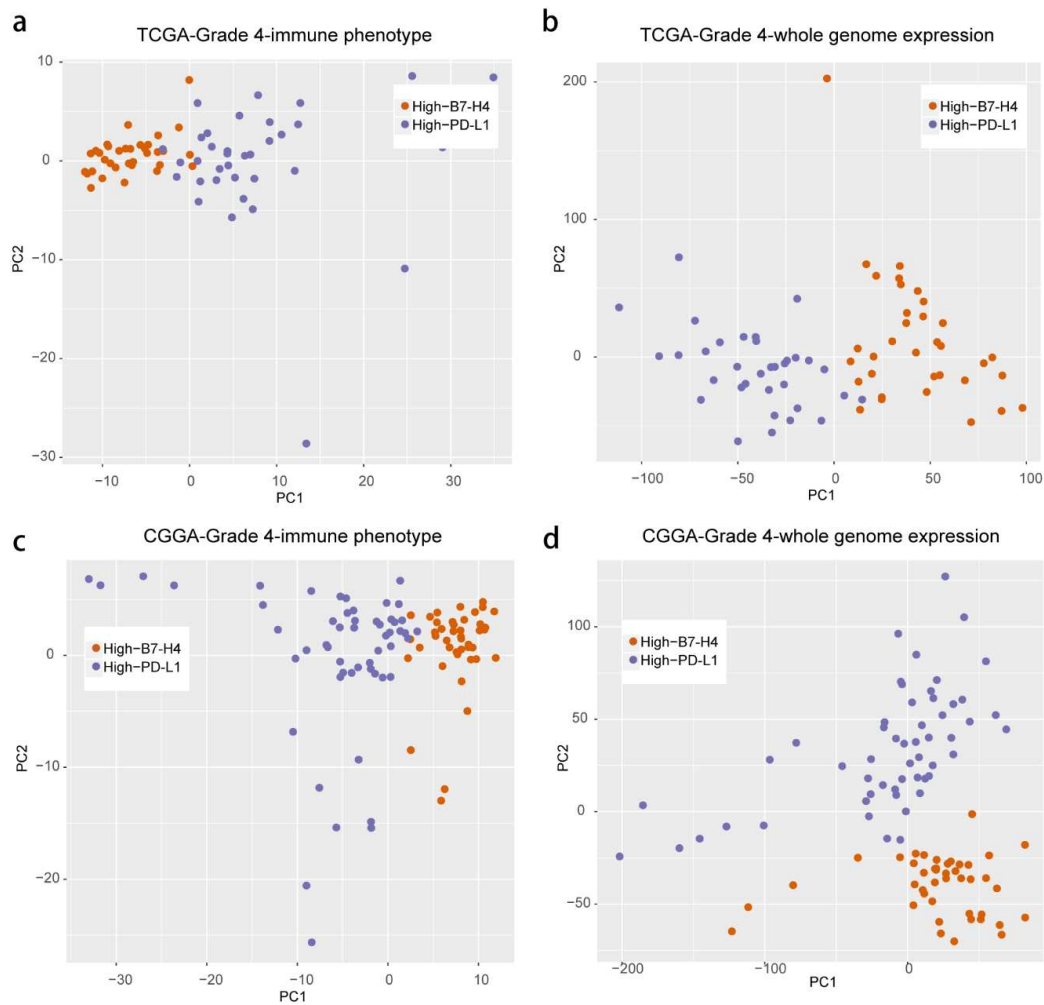
Fig. S29. Principal component analysis between High-PD-L1 and High-B7-H4 modules verified distinct immune phenotypes and whole genome expression profile in grade4 gliomas. Immune phenotype in grade 4 gliomas from TCGA dataset **(a)**. Whole genome expression profile in grade 4 gliomas from TCGA dataset **(b)**. Immune phenotype in grade 4 gliomas from CGGA dataset **(c)**. Whole genome expression profile in grade 4 gliomas from CGGA dataset **(d)**.
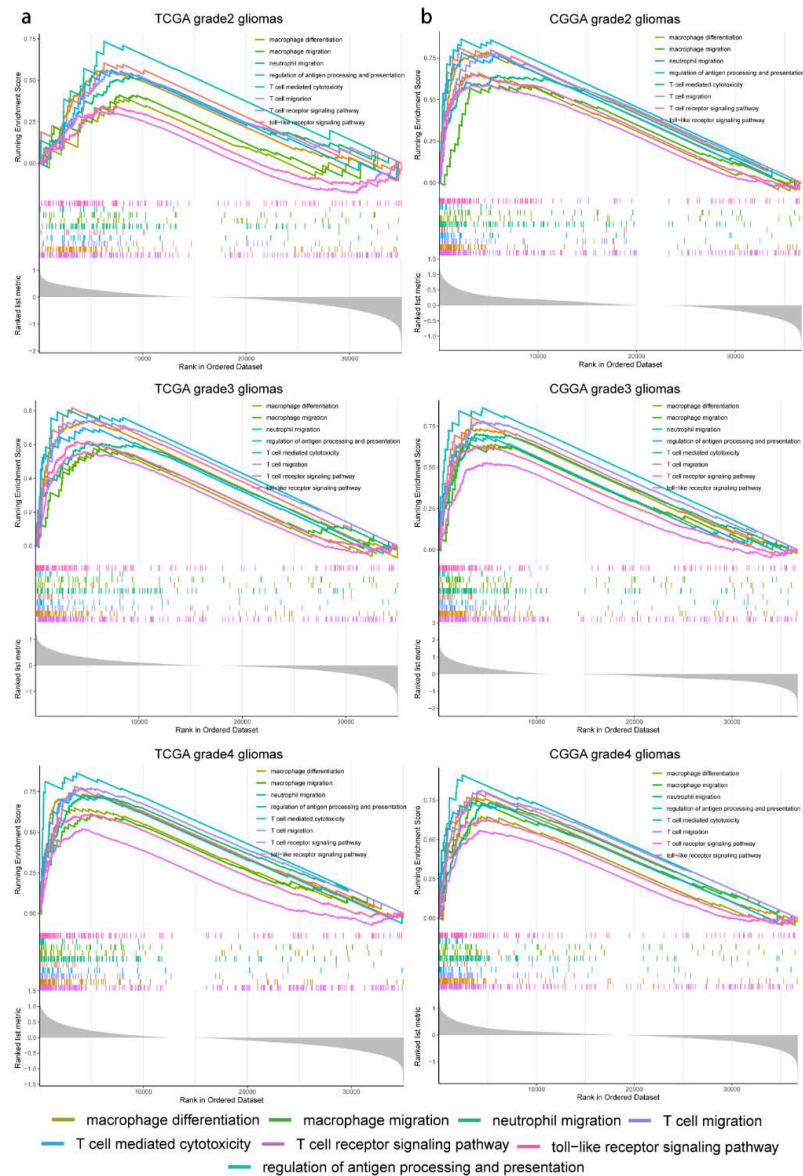
Fig. S30. GSEA analysis between High-PD-L1 and High-B7-H4 modules in each glioma grade verified High-PD-L1 module gliomas were equipped with greater immune responses. Representative GSEA results within each glioma grade in TCGA dataset **(a)**. Representative GSEA results within each glioma grade in CGGA dataset **(b)**. All of the biological processes presented here were significant difference (P< 0.01).
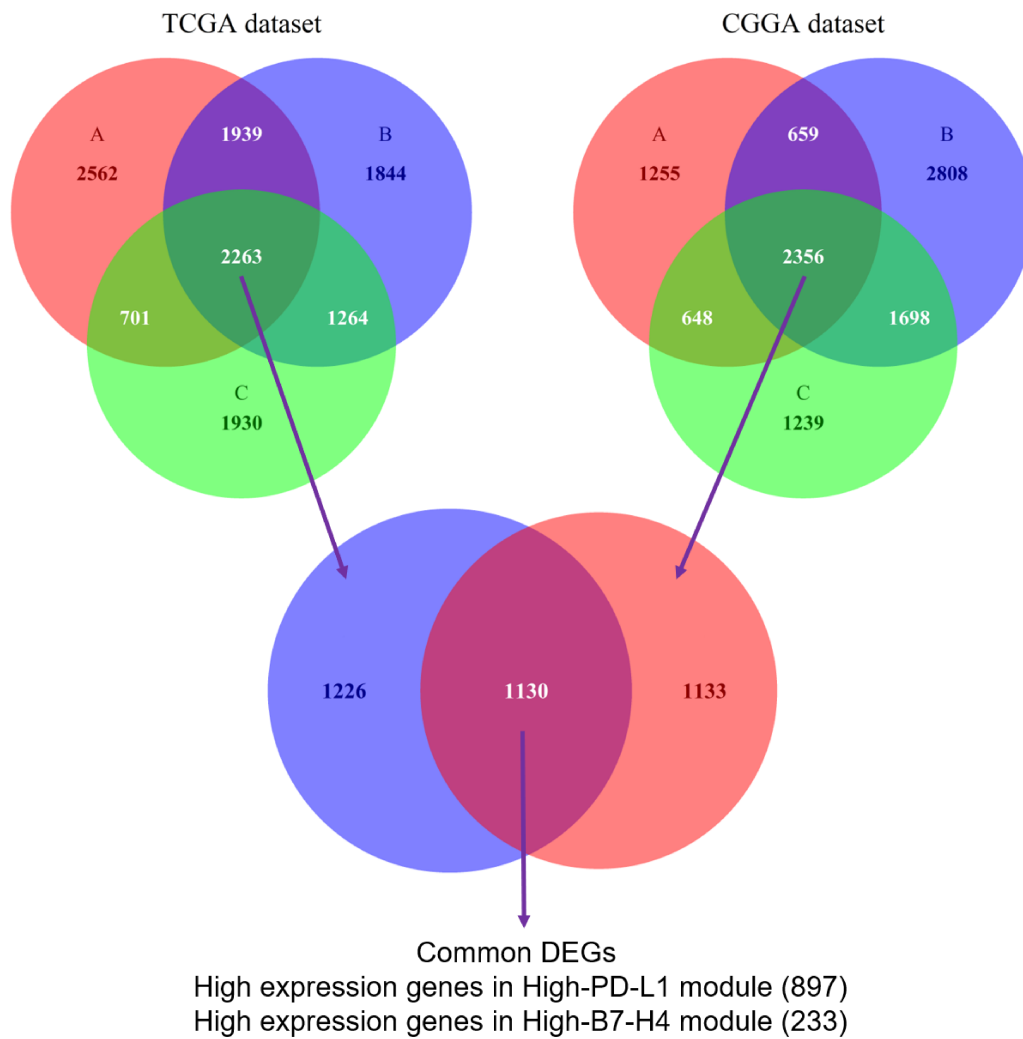
Fig. S31. Differentially expressed genes were obtained in each glioma grade from two datasets between High-PD-L1 module and High-B7-H4 module with DESeq2 package. Grade2 gliomas (A), Grade3 gliomas (B), Grade4 gliomas (C).
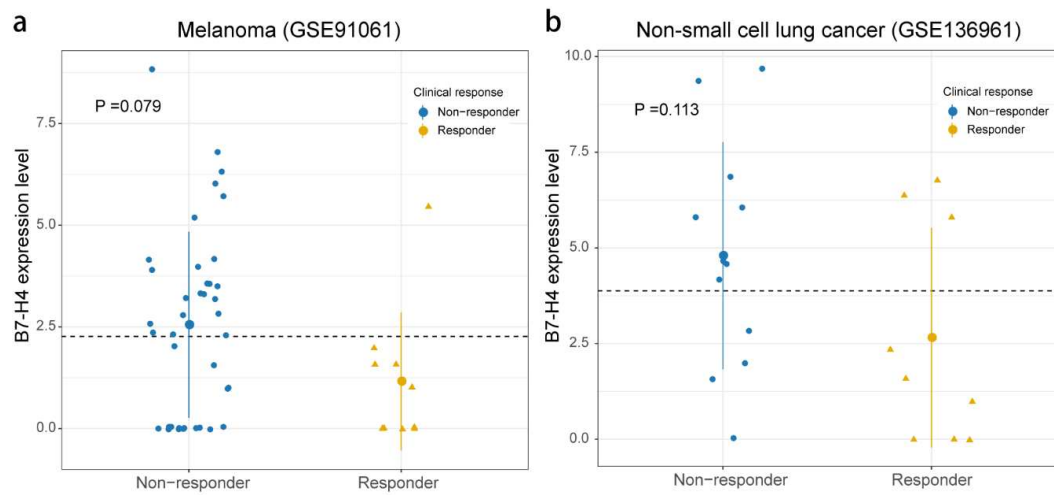
Fig. S32. Correlation between B7-H4 and survival of solid tumor patients treated with anti-PD-1 antibodies immunotherapy. Comparison of B7-H4 mRNA expression level between responders and non-responders treated with anti-PD-1 antibody in melanoma **(a, n=49)** and non-small cell lung cancer **(b, n=21)** using RNA-seq data.
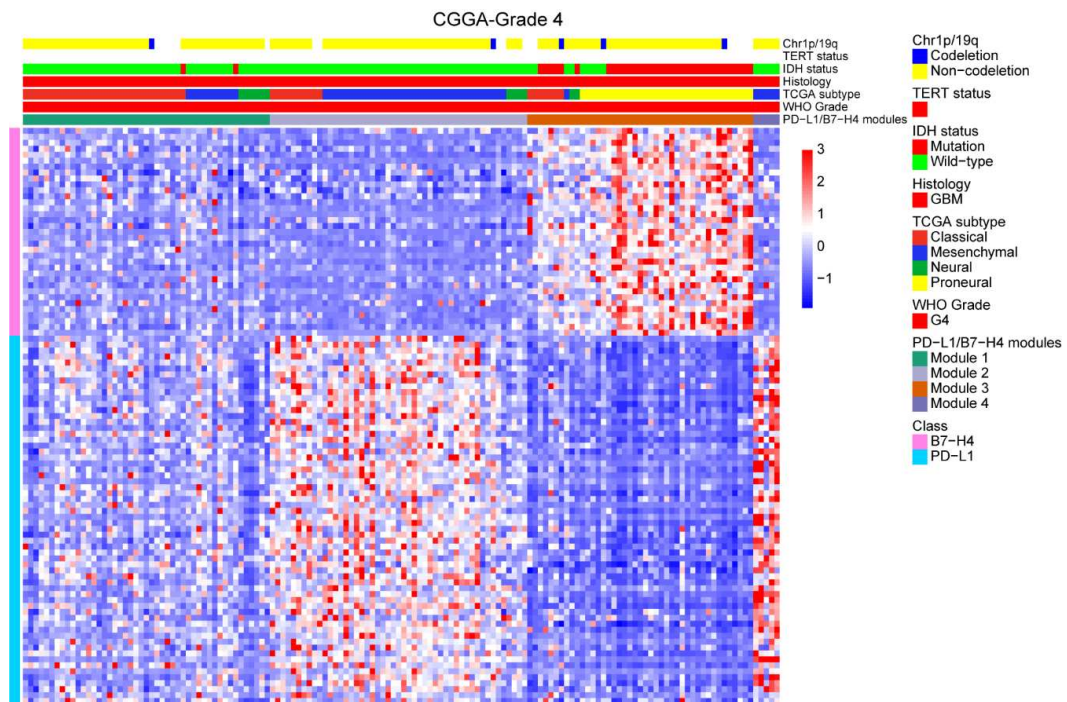
Fig. S33. Gene co-expression modules in the grade 4 gliomas from CGGA dataset showed mutually exclusive expression profiles. The module2 and module 4 were recombined into the High-PD-L1 module.